IEEE Access
Multidisciplinary | Rapid Review | Open Access Journal

Received 19 December 2023, accepted 6 January 2024, date of publication 10 January 2024,
date of current version 19 January 2024.

Digital Object Identifier 10.1109/ACCESS.2024.3352444

RESEARCH ARTICLE

Performance Enhancement of Lead-Free $CsSnI_3$ Perovskite Solar Cell: Design and Simulation With Different Electron Transport Layers

MD. FERDOUS WAHID[1], (Graduate Student Member, IEEE), MD. SHAHRIAR RAHMAN[1], (Student Member, IEEE), NOWSHAD AHMED[1], ABDULLAH AL MAMUN[1], MD. NURALAM HOWLADER[1], TARPAN PAUL[2], MD. MOTIUR RAHMAN TAREQ[1], MD. SAZEDUR RAHMAN[1], (Graduate Student Member, IEEE), AND MD. MIZANUR RAHMAN[1]

[1]Department of Electrical and Electronic Engineering, Hajee Mohammad Danesh Science and Technology University, Dinajpur 5200, Bangladesh
[2]Institute of Information and Communication Technology (IICT), Dhaka University of Engineering and Technology, Gazipur 1707, Bangladesh

Corresponding author: Md. Ferdous Wahid (mfwahid26@gmail.com)

ABSTRACT $CsSnI_3$ is a promising lead-free material that shows potential as a substitute for lead-based material in the development of ecologically benign perovskite solar cells (PSCs) due to its low cost, high efficiency, and excellent thermal stability. This research is intended to enhance the efficiency of $CsSnI_3$-based PSCs by employing numerical simulation through the One Dimensional Solar Cell Capacitance Simulator (SCAPS-1D) to optimize the optoelectronic properties of the electron transport layer (ETL), absorber layer, hole transport layer (HTL), and different interface layers. An investigation was conducted to evaluate the influence of different ETLs namely WS_2, ZnSe, C_{60} and PCBM on the performance of $CsSnI_3$-based PSCs utilizing poly (3-hexylthiophene-2,5-diyl) (P3HT) as the HTL. Moreover, the influence of variations in the thickness, doping density, and defect density of the absorber layer, ETL, and HTL on key photovoltaic parameters including power conversion efficiency (PCE), short-circuit current density (J_{SC}), open circuit voltage (V_{OC}), and fill factor (FF) was observed. The findings revealed that depending on the ETL employed, the PCE varies between the structures. For structures using WS_2, ZnSe, C_{60}, and PCBM as ETL, the corresponding PCE values are 31.63%, 29.64%, 29.75%, and 29.62%. Additionally, for all PSC structures, the effects of interface defect, temperature, series-shunt resistance, capacitance-voltage characteristics, and Mott-Schottky plot have been observed, and the corresponding current density-voltage (J-V), quantum efficiency (QE), generation, and recombination rates have been computed. Finally, the outcomes of this analysis were compared with prior research conducted on $CsSnI_3$-based PSCs, thereby offering significant perspectives for their advancement and commercial viability.

INDEX TERMS Lead-free, $CsSnI_3$, perovskite solar cell, photovoltaic cells, PSCs, ETL, HTL, SCAPS-1D.

I. INTRODUCTION

Conventional energy sources including gas, oil, and coal are being used to meet the enormous demand for Power, despite their contributions to environmental pollution and climate change [1]. However, the supply of these sources is also limited [2]. Therefore researchers are consistently working to find ways to migrate from conventional energy sources to renewable ones like hydropower, solar, wind, etc. Among them, solar energy can be a great alternative due to its free availability, excellent harvestability, and higher energy recovery rate [3]. Solar cell (SC) exploits the fundamental principles of the photoelectric effect in order to transform solar energy into electrical energy [4]. Currently, commercially viable silicon-based solar cells are available, yet their PCE is constrained to a maximum of 26% [5].

The associate editor coordinating the review of this manuscript and approving it for publication was Xiaodong Liang.

In order to alleviate this constraint, PSCs have emerged as a prominent candidate within a variety of diverse SC types for their advantageous characteristics such as tunable bandgaps, prolonged diffusion length, superior performance in carrier transfer, and simplified manufacturing processes [6]. Lead-centered PSCs have greatly improved in efficiency since 2009 [7], increasing from 3.8% to 25.8% in 2022 [8]. Although lead-centered PSCs have advantages in terms of efficiency, concerns regarding lead (Pb) toxicity and related environmental impacts persist. This has led to a noticeable increase in the interest of researchers in lead-free perovskites. However, tin (Sn) stands among a group of non-toxic or low-toxicity elements, including germanium, selenium, and antimony, that possess potential as substitutes for lead within perovskite compositions [9]. Sn-based perovskites have similar optoelectronic characteristics to Pb but exhibit better carrier mobilities, smaller band gaps, and lower toxicity. $CsSnI_3$, an entirely inorganic perovskite, possesses a band gap of 1.3 eV and exhibits optoelectronic properties that closely resemble those of its lead-based counterpart.

Numerous investigations have revealed the remarkable PV performance exhibited by $CsSnI_3$ [10], [11], [12], [13], [14], [15], [16], [17], [18], [19], [20]. The presented PSC utilizes $CsSnI_3$ as the absorber layer within a Schottky SC configuration. This pioneering study achieved a PCE of 0.9% [11]. An innovative photovoltaic quantum dot solar (PVQD) cell utilizing $CsSnI_3$ perovskite has demonstrated noteworthy PCE of 5.03% through experimental assessment [12]. Similarly, the integration of a mixed ETL with a $CsSnI_3$ absorber yielded an enhanced efficiency of 6.08% [13]. In a separate investigation, a $CsSnI_3$ PSC incorporating mesoporous metal oxide achieved a remarkable PCE of 7.50% [14]. Notably, the utilization of Black-orthorhombic $CsSnI_3$ material in the SC led to a significant advancement, resulting in a PCE of 10.1% [15]. Subsequently, lead-free $CsSnI_3$ quantum rods achieved a notable PCE of 12.96% in PV applications under AM 1.5G conditions. This technique improves light absorption and charge extraction in the perovskite phase. This lead-free $CsSnI_3$ perovskite is synthesized using a solvothermal process [16]. Concurrently, a proposed solar cell based on $CsSnI_3$ with TiO_2 as the electron transport layer (ETL) demonstrated an enhanced efficiency of 20.13% [17]. In another study, focusing on the realm of melt-synthesized $CsSnI_3$-based PSCs, a projected PCE of 23% was anticipated [18]. Moreover, $CsSnI_3$ with various charge transport layers was numerically simulated and discovered a maximum PCE of 24.73% [19]. Most recently, a numerical analysis of β-γ-$CsSnI_3$ was conducted and found a PCE value of 28.76% [20]. All of the aforementioned investigations unequivocally support the promise of $CsSnI_3$ PSCs in terms of PCE, while also demonstrating long-term thermal stability as well as illustrating the influence of various charge transport layers on photovoltaic (PV) key parameters.

In this study, lead-free $CsSnI_3$-based optimized PSC having Al/FTO/ETL/$CsSnI_3$/P3HT/Au architecture is presented that incorporates suitable ETLs to effectively enhance its PV efficacy. P3HT has been selected as the HTL in the proposed PSC for its excellent hole mobility, cost-effectiveness, and stability [21]. While TiO_2 is a widely adopted ETL for PSCs, it exhibits limitations such as lower charge mobility and instability in the U-V region [22], prompting the exploration of alternative ETL materials. The device structure under investigation encompassed four different ETLs, namely WS_2, ZnSe, C_{60}, and PCBM. ETL in PSCs facilitates electron extraction and transport, preventing electrical shunts as well as potential reactions between transparent conducting oxide (TCO) and perovskite layer, and ideally possesses high electron mobility and hole-blocking capabilities. Subsequently, across four configurations, the effects of the absorber, HTL and ETL thickness, doping density, defect density, interface defects, series-shunt resistance, and temperature on key performance parameters of PSC were thoroughly analyzed. Furthermore, this study explores the properties of capacitance-voltage relationship (C-V), generation-recombination rate, J-V Curve and QE in order to improve the performance of PSCs based on $CsSnI_3$ by appropriate integration of the ETL.

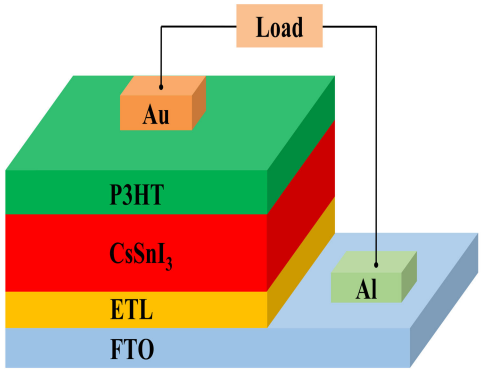

FIGURE 1. Schematic structure of the designed PSC.

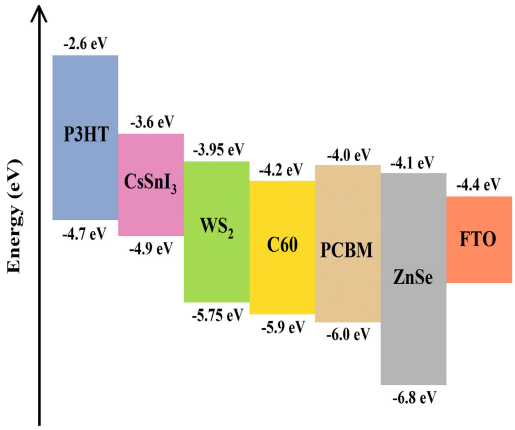

FIGURE 2. Materials energy band alignment.

II. DEVICE DESIGN AND SIMULATION

A. PROPOSED $CsSnI_3$ PSC ARCHITECTURE

In the designed PSC structure (Al/FTO/ETL/$CsSnI_3$/P3HT /Au), illustrated in Figure 1, $CsSnI_3$ functions as the absorber layer, significantly impacting the PV parameters due to

TABLE 1. Input parameters of various layers used in simulation.

Parameters	FTO [23], [24]	P3HT [25], [26]	$CsSnI_3$ [3], [27]	WS_2 [28]–[30]	ZnSe [31], [32]	C_{60} [33]	PCBM [34]
Thickness (μm)	0.5	0.05-0.5	0.4-1.2	0.03-0.5	0.03-0.5	0.03-0.5	0.03-0.5
Band gap (eV)	3.5	2	1.3	1.8	2.7	1.7	2
Affinity (eV)	4	3.2	3.9	3.95	4.09	3.9	3.9
Dielectric Permittivity	9	4.2	18	13.6	10	4.2	3.9
CB effective DOS (cm^{-3})	2.2×10^{18}	2×10^{21}	2.2×10^{17}	1×10^{18}	1.5×10^{18}	8×10^{19}	2.5×10^{21}
VB effective DOS (cm^{-3})	1.8×10^{19}	2×10^{21}	1.8×10^{19}	2.4×10^{19}	1.8×10^{19}	8×10^{19}	2.5×10^{21}
Electron mobility ($cm^2\ Vs^{-1}$)	20	1.8×10^{-3}	1500	1×10^{7}	50	100	0.2
Hole mobility ($cm^2\ Vs^{-1}$)	10	1.8×10^{-3}	585	1×10^{7}	20	25	0.2
Donor Density (cm^{-3})	1×10^{17}	0	0	10^{15}-10^{20}	10^{15}-10^{20}	10^{15}-10^{20}	10^{15}-10^{20}
Acceptor Density (cm^{-3})	0	10^{14}-10^{20}	10^{11}-10^{18}	0	0	0	0
Defect Density (cm^{-3})	1×10^{15}	10^{12}-10^{18}	10^{11}-10^{18}	10^{11}-10^{17}	10^{11}-10^{17}	10^{11}-10^{17}	10^{11}-10^{17}

TABLE 2. Input parameters of interface and bulk defect [35], [36].

Parameter	FTO/ETL Interface	ETL/$CsSnI_3$ Interface	$CsSnI_3$/HTL Interface	Bulk $CsSnI_3$
Defect type	neutral	neutral	neutral	neutral
Total Defect Density (cm^{-3})	1×10^{11}	10^{10} - 10^{18}	10^{11} - 10^{20}	10^{11}- 10^{18}
Electron capture cross section (cm^2)	1×10^{-19}	1×10^{-19}	1×10^{-19}	1×10^{-15}
Hole capture cross section (cm^2)	1×10^{-19}	1×10^{-19}	1×10^{-19}	1×10^{-15}
Energy distribution	Gaussian	Gaussian	Gaussian	Gaussian
Reference defect energy level	0.6	0.6	0.6	0.6

its optical absorption characteristics. The PSC architecture employs P3HT and fluorine-doped tin oxide (FTO) as HTL and TCO, respectively, with Aluminum (Al) and Gold (Au) serving as front and rear contacts. Four different ETL materials, specifically WS_2, ZnSe, C_{60}, and PCBM were employed in the study. The interaction between ETL and HTL has a significant influence on the transportation and extraction of charges produced in the absorber layer, hence affecting key parameters such as V_{OC}, PCE, FF, and J_{SC}. The V_{OC} is influenced by the disparity in Fermi energy levels between the ETL and HTL. Additionally, the enhanced charge mobility of the ETL leads to a commensurate increase in the FF and J_{SC}. The successful extraction of holes is facilitated by the combination of high hole mobility and suitable ionization potential of the HTL. Consequently, the parameters of ETL and HTL play significant roles in enhancing the overall performance of PSCs. The band diagram of the PSC device configuration based on $CsSnI_3$ is depicted in Figure 2.

B. NUMERICAL SIMULATION APPROACH

In this research work, the designed PSC architectures were numerically analyzed by employing Solar Cell Capacitance Simulator (SCAPS-1D) software. SCAPS-1D is a program that can be used to model SCs in a single dimension. It was created at the Department of Electronics and Information Systems (ELIS) at the University of Gent in Belgium. It has the capability to accommodate a maximum of seven distinct layers. These layers consist of six interface layers and two electrodes [37]. The software performs computations to determine PV parameters (PCE, FF, V_{OC} and J_{SC}) by leveraging the Poisson equation, continuity equation, and current density equation. Equation (1) represents Poisson's equation that establishes the connection between the electrostatic potential and the distribution of charge density. The continuity equations for electrons and holes can be expressed mathematically as (2) and (3), respectively. The computation of electron and hole current densities was conducted utilizing

(4) and (5), respectively.

$$\frac{\partial^2 \psi}{\partial x} = -\frac{\partial E}{\partial x} = -\frac{\rho}{\varepsilon_s} = -\frac{q}{\varepsilon_s}\left[\mathrm{p} - \mathrm{n} + N_{\mathrm{D}}^{+}(x) - N_{\mathrm{A}}^{-}(x) \pm N_{\mathrm{def}}(x)\right] \tag{1}$$

$$\frac{\partial j_{\mathrm{n}}}{\partial x} + G_{\mathrm{n}} - U_{\mathrm{n}}(\mathrm{n}, \mathrm{p}) = 0 \tag{2}$$

$$-\frac{\partial j_{\mathrm{p}}}{\partial x} + G_{\mathrm{p}} - U_{\mathrm{p}}(\mathrm{n}, \mathrm{p}) = 0 \tag{3}$$

$$j_{\mathrm{n}} = q\mathrm{n}\mu_{\mathrm{n}}E + qD_{\mathrm{n}}\frac{\partial \mathrm{n}}{\partial x} \tag{4}$$

$$j_{\mathrm{p}} = q\mathrm{p}\mu_{\mathrm{P}}E - qD_{\mathrm{P}}\frac{\partial P}{\partial x} \tag{5}$$

where electric field, charge density, charge of electron, electrostatic potential, relative permittivity, electron/hole concentration, and rate of electron/hole generation is represented by E, ρ, q, ψ, ϵ, n/p, G_n/G_p respectively. Also, $N_D{}^+/N_A{}^-$ represents ionized donor/acceptor density, D_p / D_n represents the coefficient of diffusion for hole/electron, U(n,p) denotes the overall recombination rate, μ_p/μ_n denotes hole/electron mobility [38], [39]. The numerical simulation of the designed PSCs was performed under controlled parameters, including a solar radiation intensity of 100 mW/cm^2, a radiation frequency of 1MHz and AM 1.5G solar spectrum. These conditions are maintained at an operating temperature of 300K. The incident light is postulated to originate from the top of TCO, specifically FTO, which has a work function of 4.4 eV. The rear contact is constructed from gold (Au) and exhibits a work function of 5.1 eV. In accordance with previous simulation outcomes, the thickness of the FTO layer was established at 0.5 μm [40]. During the optimization of a specific parameter, the other parameters were maintained constant. Table 1 presents the optoelectronic properties of the materials employed in this study during SCAPS-1D simulation and Table 2 demonstrates the input parameters related to interface defect. At room temperature, the thermal velocity for electrons and holes within each layer is considered to be 10^7 cm/s, influencing mobility and recombination dynamics. The improvement of carrier collecting efficacy can be achieved through the enhancement of thermal velocities. However, it is important to note that this enhancement may also lead to an increase in recombination rates. Consequently, the diffusion length can be affected, which in turn has a negative impact on PCE [41].

III. RESULTS AND DISCUSSION

A. IMPACT ON PV PARAMETERS FOR THE VARIATION OF ABSORBER DEFECT DENSITY AND THICKNESS

The performance of $CsSnI_3$-based PSCs is greatly influenced by the variation in thickness and defect density of the absorber layer. This is because they directly impact light absorption and the generation of charge carriers within the absorber layer. Specifically, a thinner absorber layer usually results in reduced sunlight absorption, as it accommodates fewer photons, potentially diminishing PCE. On the contrary, PCE may rise as a result of improved light absorption from a thicker layer. However, excessive thick layer can also lead to greater electron-hole recombination and impede charge transport, lowering the efficiency. Additionally, thicker layers may also have an impact on mechanical stability and manufacturing consistency. Furthermore, defects are more prone to emerge in thicker absorber layer, reducing SC efficiency to a greater extent. High defect density results in low carrier diffusion length and a high recombination process, which lead to lower PV performance [42]. Therefore, it is a must to investigate optimal defect density in relation to absorber layer thickness. For this reason, the thickness was varied from 0.4 μm to 1.2 μm while the total defect density ranged from 10^{11} cm^{-3} to 10^{18} cm^{-3}, concurrently. The contour plots in Figure (3-6) show that the PV parameters varied in a very similar way across all of the ETL. The V_{OC} of WS_2, ZnSe, C_{60} and PCBM has drastically decreased from 1.21 V to 0.87 V, 1.10 V to 0.78 V, 1.18 V to 0.87 V and 1.11 V to 0.802 V respectively. These structures showed that V_{OC} values are highest when defect density is less than 10^{17} cm^{-3} and thickness is between 0.4 μm to 0.9 μm. This variance in V_{OC} is attributable to longer diffusion length and higher carrier lifespan within the specified range [43]. However, the structure with WS_2 ETL had the highest V_{OC} value, while the one with ZnSe ETL had the lowest. Similar trends in J_{SC} values were seen across all four structures in Figure 4(a-d). J_{SC} starts to increase when the thickness is beyond 0.8 μm and the defect density lies below 10^{17} cm^{-3}. The rise in J_{SC} happens because as the absorber layer thickens, its effective surface area increases, allowing more light to be absorbed and creating more charge carriers [44]. Conversely, recombination driven by high defect density lowers J_{SC} above that level of defect density [45]. The J_{SC} of structures consisting of WS_2, ZnSe, PCBM and C_{60} attained approximately 31.09 mA/cm^2, 32.77 mA/cm^2, 30.85 mA/cm^2, and 32.62 mA/cm^2, respectively. Having the same variation in defect density and thickness, FF also declines from 87.86% to 84.40%, 83.75% to 69.15%, 84.54% to 80.08% and 84.42% to 76.22% for WS_2, ZnSe, C_{60} and PCBM respectively in Figure 5(a-d). Since FF is influenced by the V_{OC} and recombination rate at the depletion area, it follows the same trend as V_{OC} [46]. Further, intermediate defect densities exhibited favourable FF values for organic ETL. This may be a consequence of specific defects serving as passivators for more profound trap states [47]. In addition, ZnSe exhibits significant deterioration in the Fill Factor.

Figure 6(a-d) shows a drastic decrease in PCE of the PSCs for WS_2, ZnSe, C_{60} and PCBM from 37.40% to 21%, 32.35% to 16.75%, 32.20% to 20.15% and 32.20% to 18.90% respectively. Again, ZnSe demonstrated a higher PCE reduction rate (about 49%) than the other structures. PCE exhibits higher values for thickness over 0.6 μm and defect densities below 10^{16} cm^{-3}. A thicker absorber layer (> 0.6 μm) increases carrier production through light absorption,

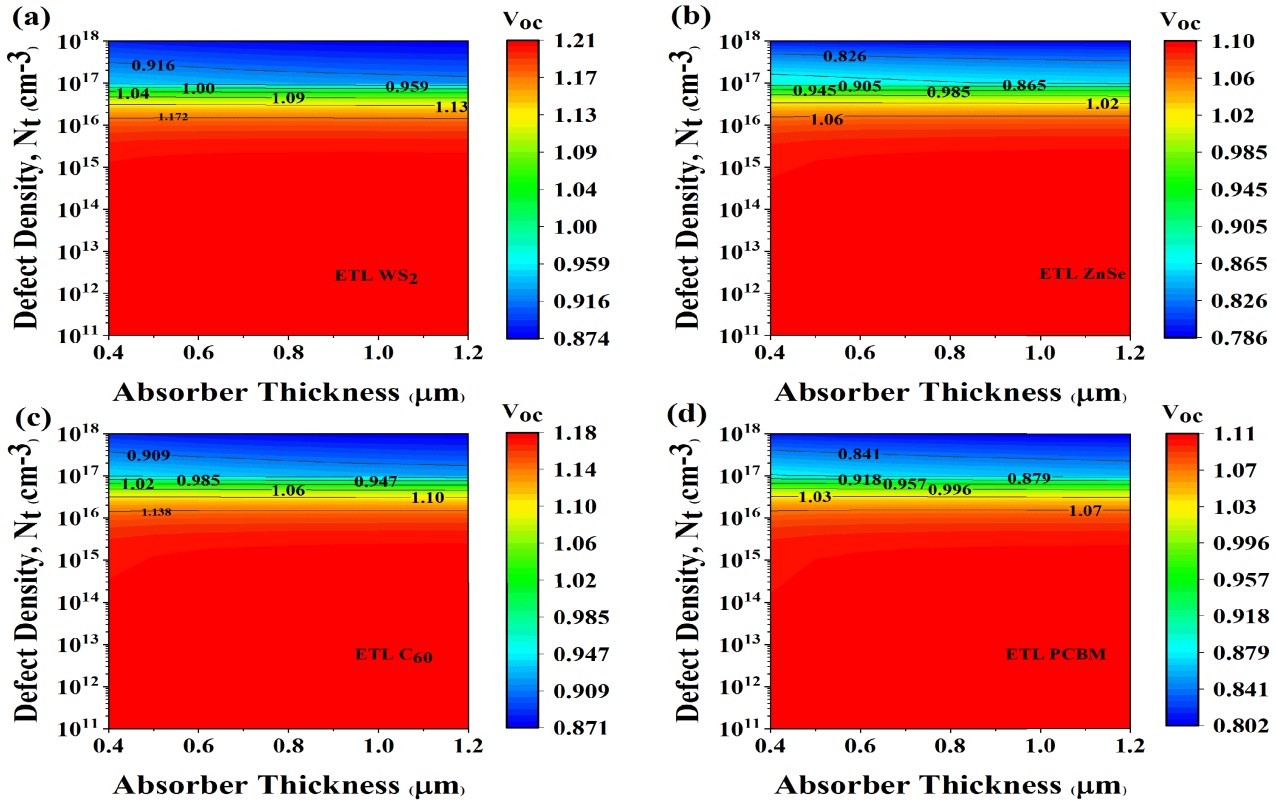

FIGURE 3. Contour plot demonstrating V_{OC} for the variation of absorber layer thickness and defect concentration using (a) WS_2, (b) ZnSe, (c) C_{60} and (d) PCBM as ETLs.

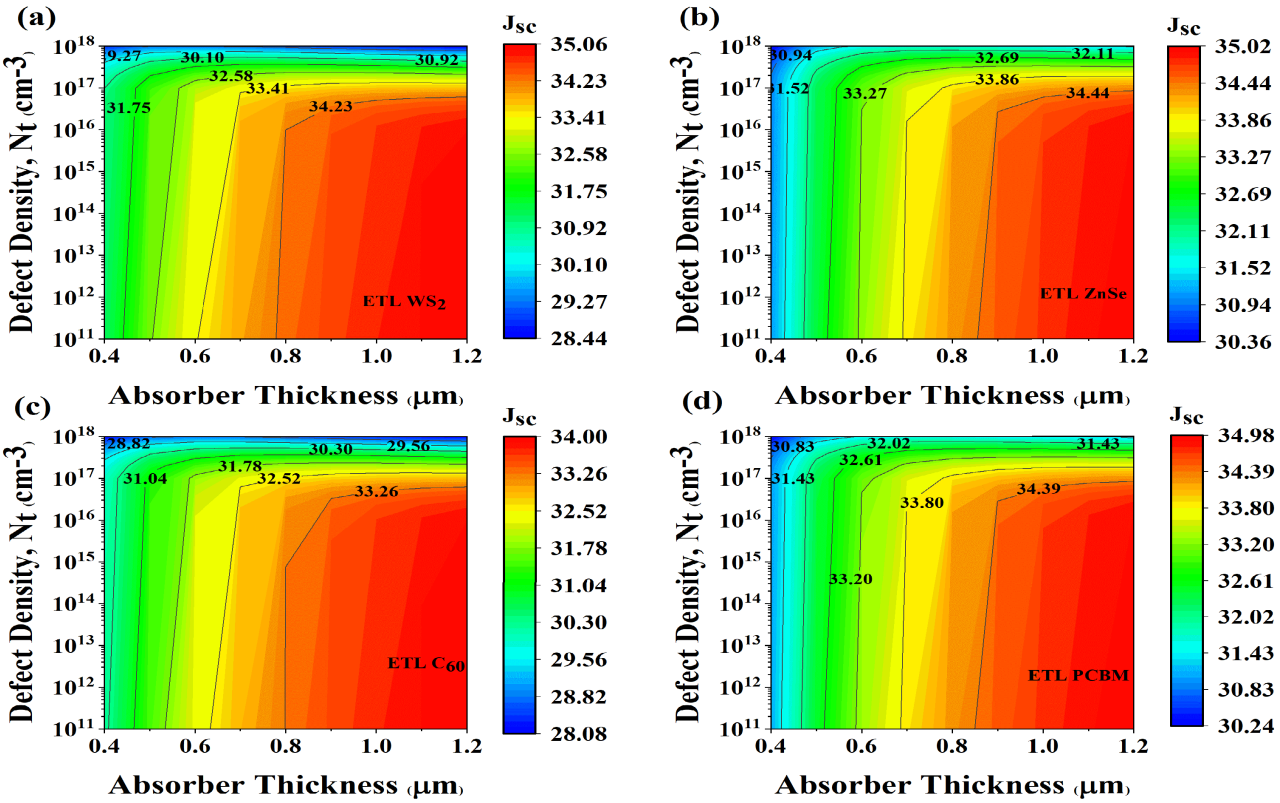

FIGURE 4. Contour plot demonstrating J_{SC} for the variation of absorber layer thickness and defect concentration using (a) WS_2, (b) ZnSe, (c) C_{60}, and (d) PCBM as ETLs.

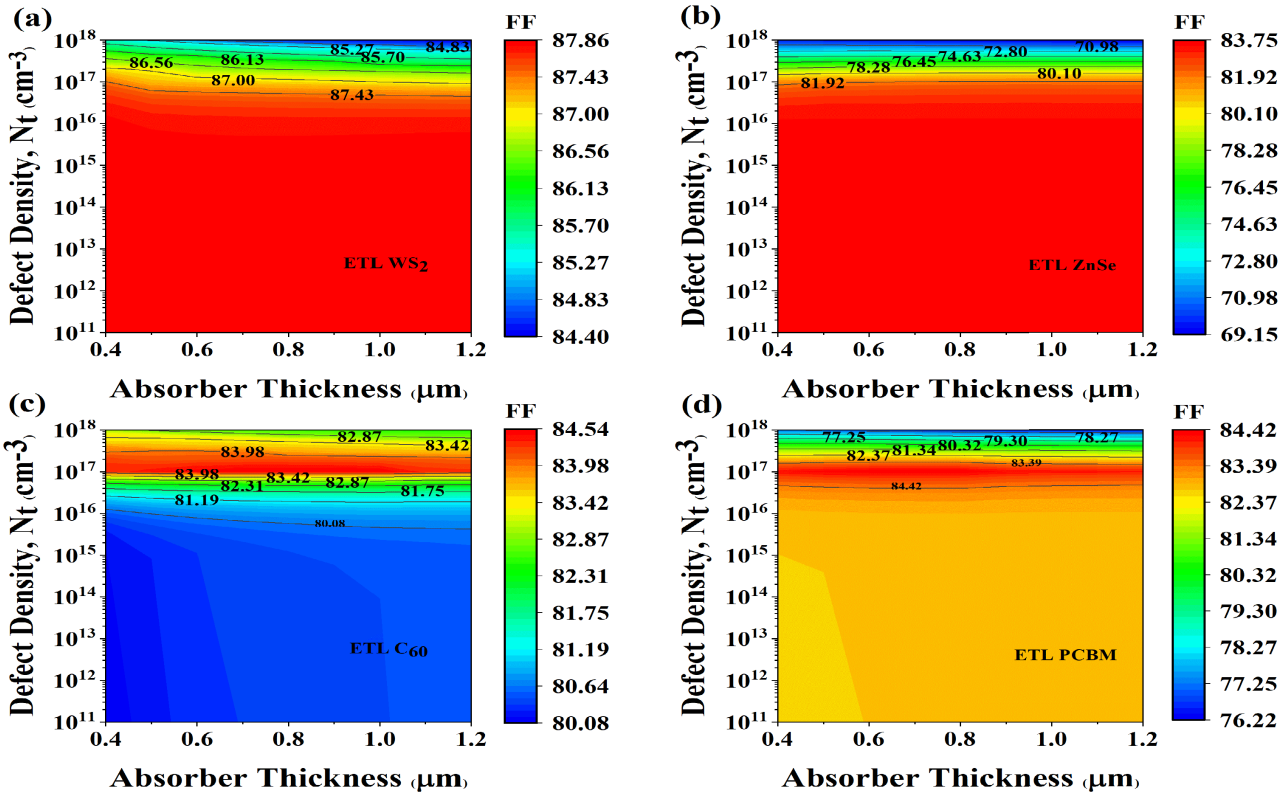

FIGURE 5. Contour plot demonstrating FF for the variation of absorber layer thickness and defect concentration using (a) WS_2, (b) ZnSe, (c) C_{60} and (d) PCBM as ETLs.

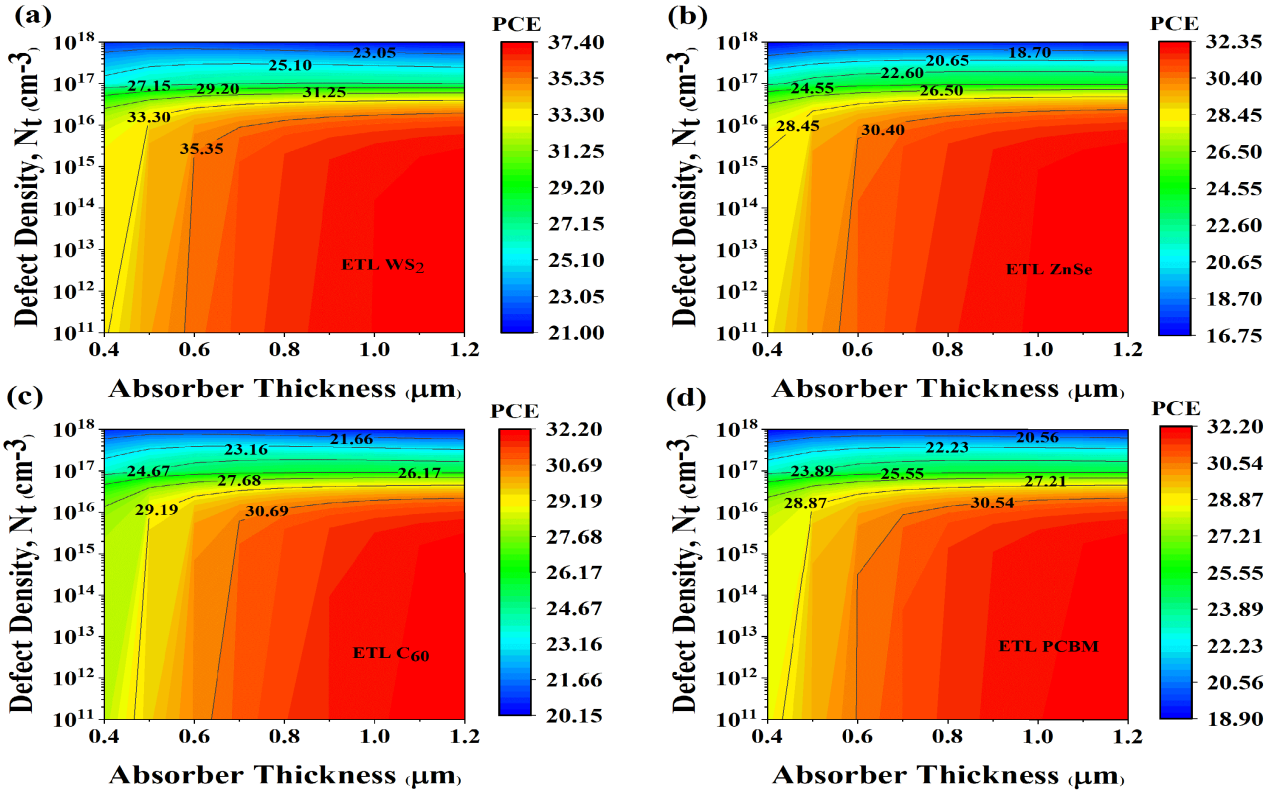

FIGURE 6. Contour plot demonstrating PCE for the variation of absorber layer thickness and defect concentration using (a) WS_2, (b) ZnSe, (c) C_{60}, and (d) PCBM as ETLs.

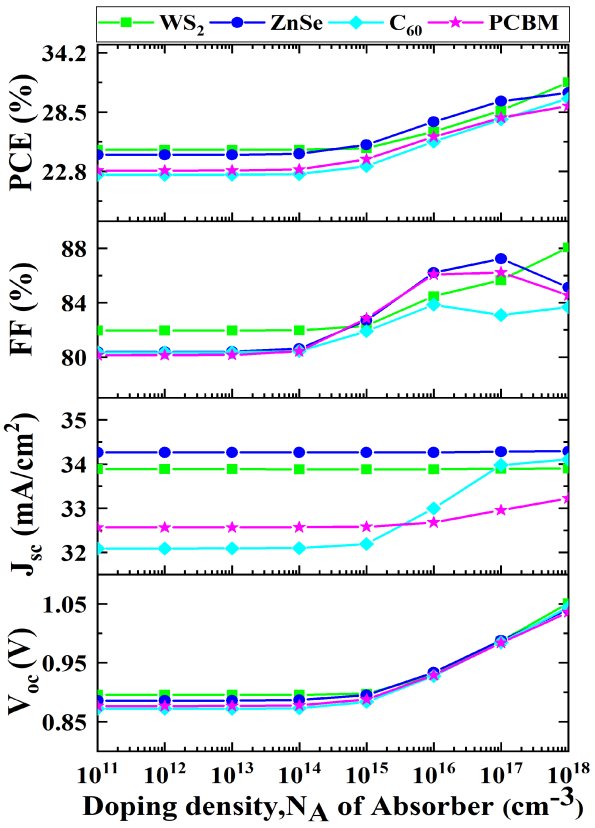

FIGURE 7. Demonstrating PV parameters for the variation of absorber layer acceptor density.

while defect density (< 10^{16} cm^{-3}) reduces non-radiative recombination. The notable PCE within the specified range of absorber layer thickness and defect density is due to the combined influence of those factors [48]. Therefore, the PV cell's overall performance has been considerably impacted by the combined factors of thickness and total defect density. Based on the aforementioned assessment, it has been determined that the ideal thickness and total defect density of the absorber layer are decided to be 0.8 μm and 10^{16} cm^{-3}, respectively, in order to provide viable properties of a proficient absorber layer.

B. IMPACT OF ABSORBER LAYER DOPING DENSITY ON PV PERFORMANCE

The efficiency of the SC can be enhanced by employing precise doping on the absorbing material [49]. However, excessive doping might be unfavorable due to its non-conventional nature, potential hindrance to the mechanism of carrier transport and increased fabrication complexity [50]. Thus, the doping concentration of the absorber was changed from 10^{11} cm^{-3} to 10^{18} cm^{-3} to determine the optimum value during the simulation. Figure 7 demonstrates that the V_{OC} of all ETL associated structure has stayed constant for N_A values up to 10^{15} cm^{-3}, and thereafter increases with the N_A. An increase in N_A lowers the Fermi energy of the holes, leading to a higher value of V_{OC} [51]. All ETLs have the same trend in PCE up to 10^{14} cm^{-3}, but after that, the PCE increases as the N_A becomes higher. The consistent J_{SC} in WS_2 and ZnSe associated structures despite varying N_A may be attributed to their limited band binding behavior. These findings are quite consistent with the SC outputs on altering the absorber doping reported in prior investigations [52], [53]. For the organic ETL based structures, J_{SC} remains constant up to 10^{15} cm^{-3} and then increases as N_A rises due to improved band alignment. FF stays the same up until 10^{14} cm^{-3} for all of the ETLs, after which it starts to rise in a different manner. Since absorber doping has had a profound impact throughout the simulation, choosing an appropriate acceptor doping concentration is crucial for maximizing device performance [54]. Optimal N_A of the absorber layer is established at 10^{18} cm^{-3}, 10^{17} cm^{-3}, 10^{16} cm^{-3} and 10^{17} cm^{-3} for the WS_2, ZnSe, C_{60} and PCBM ETLs respectively, considering the superior performance in PCE and FF.

C. EFFECT OF ETL LAYER THICKNESS, DOPING, AND DEFECT ON PV PERFORMANCE

1) EFFECT OF ETL LAYER THICKNESS

ETL performs an indispensable role in electron extraction from the absorber layer [55]. In the current study, the thickness of WS_2, ZnSe, C_{60} and PCBM as ETL layer was varied from 0.03 μm to 0.5 μm. This is evident from Figure 8(a) that thickness has a negligible effect on the inorganic ETL i.e. WS_2 and ZnSe due to their transparent nature. A similar pattern is observed in previous literature too [56], [57]. On the contrary, there is a marginal diminution in the parameters using organic ETL i.e. C_{60} and PCBM due to the formation of larger pinholes which is identical to the previous literature [58]. There is only an exception in the FF of the C_{60}-based one as it decreases first, then increased significantly. Yue et al. reported a similar pattern for C_{60} as ETL-based structure [59]. Thus, selecting a proper ETL with optimum thickness is important. In this study, 0.03 μm is taken as the optimum thickness for further simulation.

2) IMPACT OF DOPING DENSITY OF ETL LAYER

Small amounts of impurity atoms can enhance solar cell performance [60]. The effect of changing the doping concentration (N_D) from 10^{15} cm^{-3} to 10^{20} cm^{-3} on the PV characteristics of several ETLs including WS_2, ZnSe, C_{60} and PCBM is shown in Figure 8(b). It is found that an increase in ETL doping results in a marginal enhancement in J_{SC} for all configurations which reaches saturation at 10^{17} cm^{-3}. In contrast, it exhibits almost constant progress for open-circuit voltage, Fill Factor, and PCE as doping gets higher. Therefore, it can be concluded that raising the doping level did not make any substantial improvement across all the structures in this study. A very similar pattern has been documented in prior research studies [61]. For the purpose of further optimization, the value of N_D was set as 10^{17} cm^{-3}.

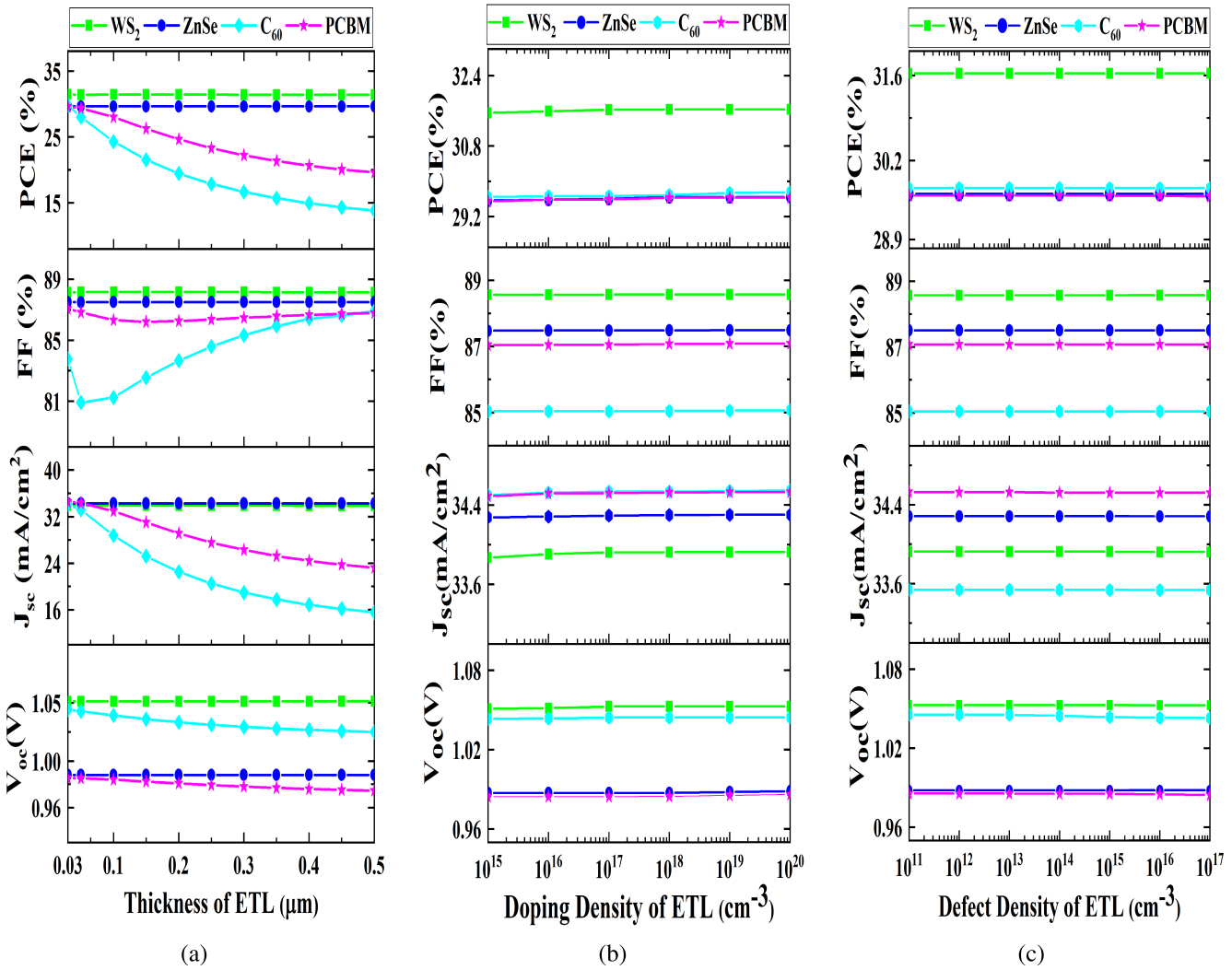

FIGURE 8. Demonstrating PV parameters for the variation of (a) ETL thickness, (b) ETL donor doping density, and (c) ETL defect density.

3) IMPACT OF DEFECT DENSITY OF ETL LAYER

Figure 8(c) demonstrated that all performance parameters exhibited almost constant values across all ETL layers as defect density (N_t) increased from 10^{11} cm^{-3} to 10^{17} cm^{-3}. Thus, the repercussion of higher defect density of ETL on device configurations is negligible. The previously published work also exhibits resembling behavior [62]. The simulation disclosed that the WS_2 associated structure did not exhibit a better J_{SC} value, but it performed exceptionally well in every other parameter. With a V_{OC} of 1.0527 V, a J_{SC} of 33.923 mA/cm^2 and an FF of 88.570%, the WS_2-related structure achieved the greatest efficiency of 31.629%. On the contrary, the structure using PCBM as the ETL demonstrated the worst performance in terms of both V_{OC} and PCE, despite showing the greatest values of J_{SC} (34.529 mA/cm^2). Furthermore, it is found that the structure associated with C_{60} had the lowest fill factor of 85.04%. In this study, the optimized N_t is set to 10^{15} cm^{-3} for all four device structures.

D. EFFECT OF HTL LAYER THICKNESS, DOPING AND DEFECT DENSITY ON PV PERFORMANCE

1) EFFECT OF HTL LAYER THICKNESS

Figure 9(a) shows the output parameters with increasing HTL thickness for different combinations of ETL. The thickness was varied from 0.05 μm to 0.5 μm to obtain an optimum value. It is noticed from the figure that, V_{OC} and J_{SC} remained constant whereas there was a negligible decrease in FF and PCE. It has been previously documented by Hossain et al. [63]. This is because $CsSnI_3$ has high absorption coefficient and it is less susceptible to the thickness of the HTL layer [27]. Yet, the perovskite layer is better able to collect photons when the HTL is thicker [64]. Therefore, the thickness of HTL layer was kept at 0.1 μm for furthur optimization.

2) IMPACT OF VARIATION IN DOPING DENSITY AT HTL LAYER

Figure 9(b) demonstrates the influence of PV parameters with increasing acceptor concentration (N_A) of HTL for four

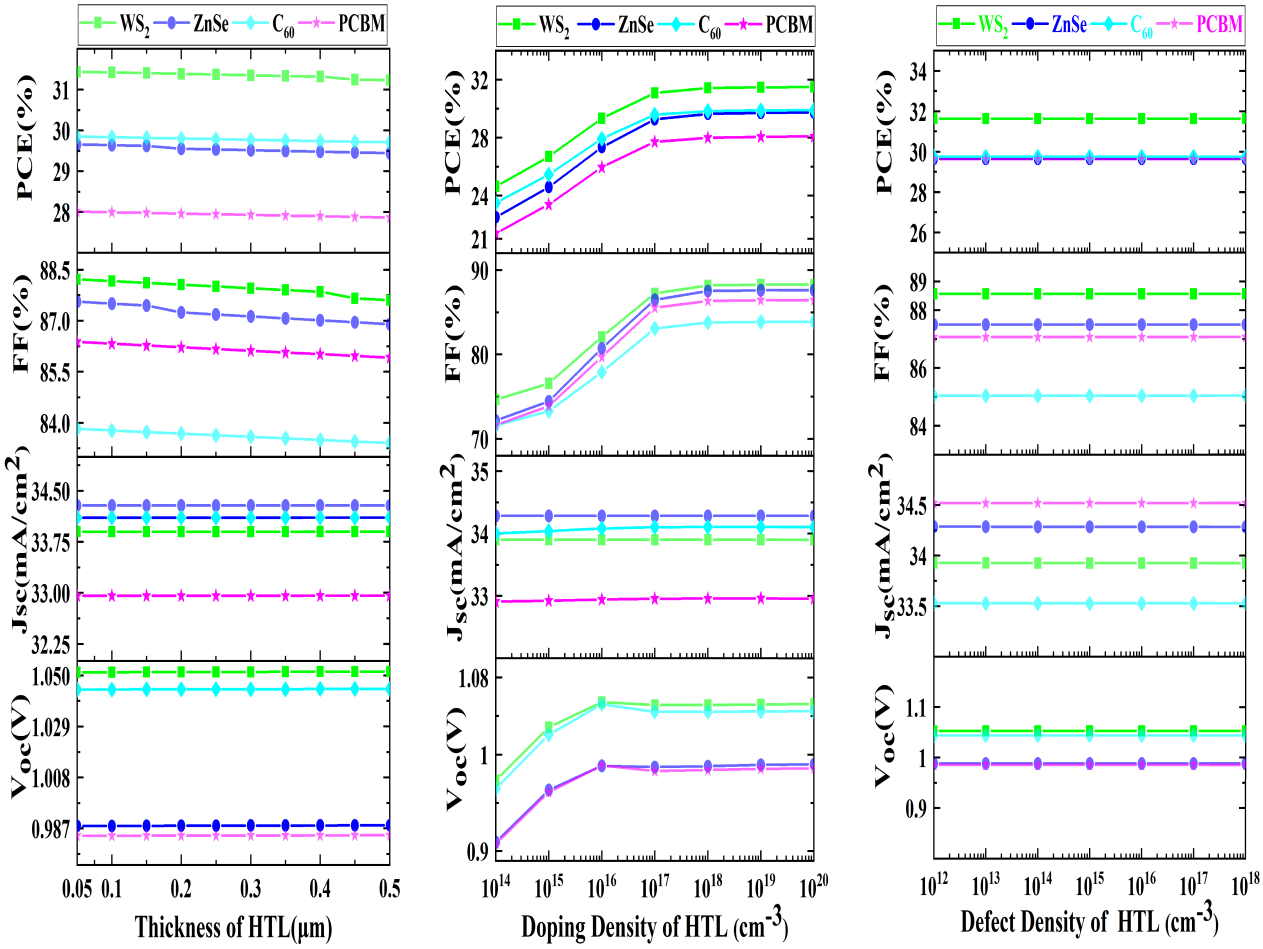

FIGURE 9. Demonstrating PV parameters for the variation of (a) HTL thickness, (b) HTL Acceptor doping density and (c) HTL defect density.

individual architectures. N_A of HTL layer was ranged from 10^{14} cm^{-3} to 10^{20} cm^{-3}. It is found from the figure that V_{OC} initially increased up to 10^{16} cm^{-3} with variation in N_A and then remained constant. A similar trend has been observed in the case of FF and PCE. Both the parameters increased decisively up to 10^{17} cm^{-3} and after that remained constant. The increase in the parameters is owing to the improvement in the electric field because it facilitates the charge carrier extraction [65]. But there was no significant change in J_{SC}.This means N_A variation of the HTLs has a negligible impact on J_{SC}. Overall, WS_2 showed the best performance. Previous studies have already mentioned a similar pattern in the SC parameters [66]. The ideal concentration of the hole transport layer was taken as 10^{17} cm^{-3} for further optimization.

3) IMPACT OF VARIATION IN DEFECT DENSITY AT HTL LAYER

Figure 9(c) shows the influence of PV parameters with increasing defect density of HTL. The density of neutral type defect was varied from 10^{12} cm^{-3} to 10^{18} cm^{-3}, while the remaining parameters were maintained at their optimized values. The value of V_{OC}, J_{SC}, FF, and PCE was almost constant throughout this variation. This may be related to the high absorption coefficient of $CsSnI_3$ or the high carrier mobility of P3HT. Previously, the same behavior was observed when the effect of HTL defect density was investigated [61], [67]. However, the optimum density was determined to be 10^{12} cm^{-3} for further simulation.

E. EFFECT OF INTERFACE DEFECT DENSITY ON PV PERFORMANCE

1) IMPACT OF DEFECT DENSITY AT HTL/$CsSnI_3$ INTERFACE

The effectiveness of solar cell is greatly influenced because of the recombination losses in the interface [68]. To investigate the influence of interface recombination occurring at interfaces between HTL and $CsSnI_3$, the defect density (N_t) had ranged from 10^{11} cm^{-3} to 10^{20} cm^{-3}. Figure 10(a) shows that the V_{OC} is almost constant up to 10^{13} cm^{-3}. Beyond this concentration, V_{OC} drops significantly for all the structures. WS_2 had the highest V_{OC} of 1.052 V, while PCBM had the lowest of 0.881 V for varying N_t. For all structures, there were no appreciable changes in J_{SC} when

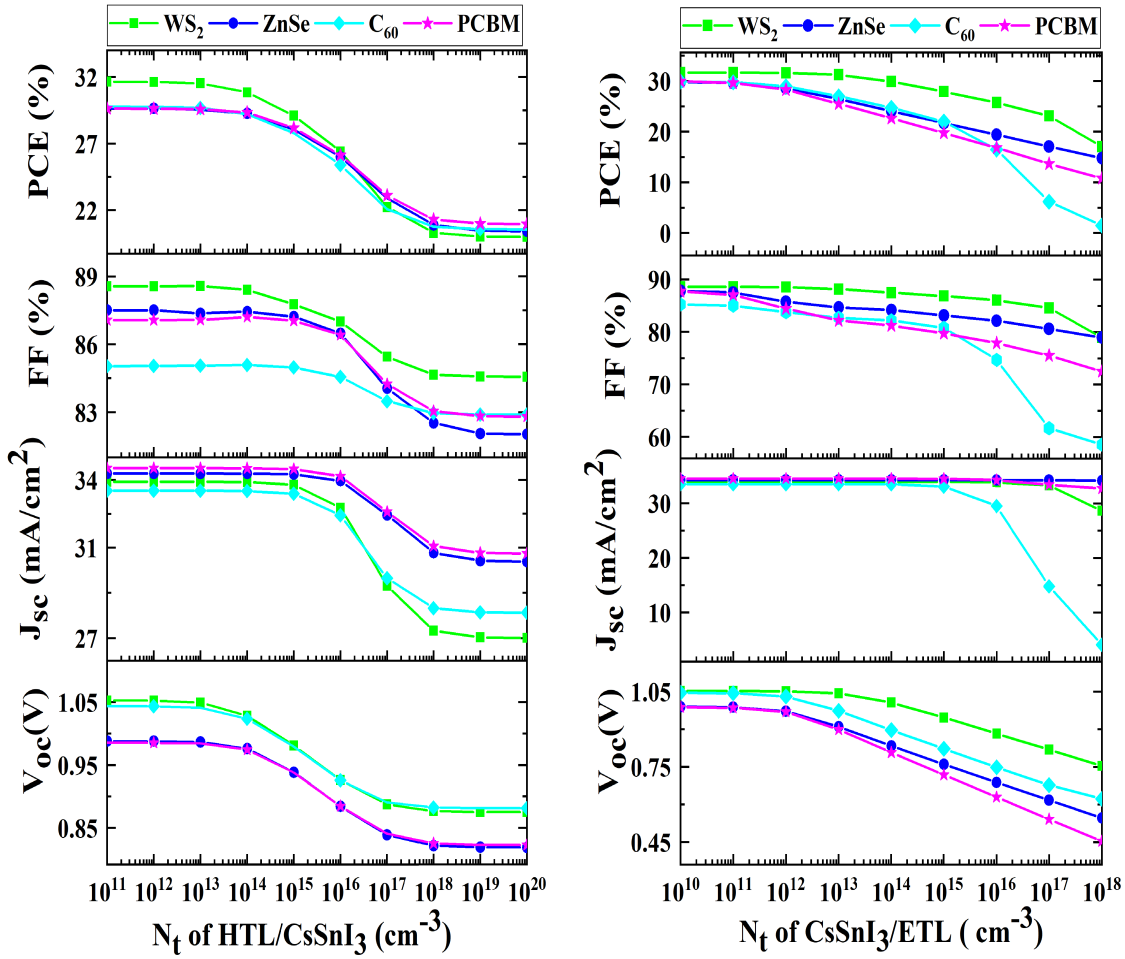

FIGURE 10. Impact of variation in interface defect density of the (a) HTL/$CsSnI_3$ and (b) $CsSnI_3$/ETL on Cell Parameters.

the defect concentration was increased up to 10^{15} cm^{-3}. J_{SC} significantly declines over this concentration. The PCE, as well as FF values, showed a similar downward trend as V_{OC} when the defect density (N_t) across HTL/$CsSnI_3$ Interface increased. Due to higher trap and recombination centers because of higher defect concentrations at the interfaces, the solar cell parameter has dramatically dropped, lowering SC performance [66]. Therefore, a value of 10^{12} cm^{-3} was set for further simulation.

2) IMPACT OF DEFECT DENSITY AT $CsSnI_3$/ETL INTERFACE

Figure 10(b) demonstrates the impact of defect density across $CsSnI_3$/ETL interface when N_t was raised from 10^{10} cm^{-3} to 10^{18} cm^{-3}. The study found that the value of V_{OC}, J_{SC}, FF, and PCE declines as N_t is raised. The V_{OC}, FF and PCE remained constant till 10^{11} cm^{-3} and then starts declining with increment in N_t. J_{SC} almost remained constant till the defect of 10^{15} cm^{-3} and then varies in a different manner. The C_{60}-associated structure had the lowest FF, J_{SC} and PCE value of 56.87%, 2.283 mA/cm^{-2} and 0.83%, respectively. In the case of V_{OC}, PCBM demonstrated the lowest value, which was less than 0.35 V. Overall, the worst tolerance against the interface defect was shown by the C_{60}-associated structure whereas ZnSe showed the best. The results also show that the V_{OC} is highly susceptible to changes in N_t compared to J_{SC}. Again, it has been found that defects in the performance of SC is affected by the ETL/$CsSnI_3$ interface more so than the $CsSnI_3$/HTL interface. Light entering the solar cell by ETL causes the front side to have a higher carrier generation and recombination rate than the back side [69]. Tan et al. observed a similar pattern [70]. However, the ideal defect density value was determined to be 10^{11} cm^{-3}, which is identical to the result obtained in prior research [71].

F. IMPACT OF PARASITIC RESISTANCES AND TEMPERATURE

1) IMPACT OF SERIES RESISTANCE (R_S)

Series resistance is a result of the PSC's internal resistance, terminal resistance and metal electrode resistance [72]. Figure 11(a) illustrates the influence of R_s affecting the performance parameters of WS_2, ZnSe, C_{60} and PCBM-based perovskite solar cells. Keeping R_{sh} set at 10^5 Ω-cm^2, R_s

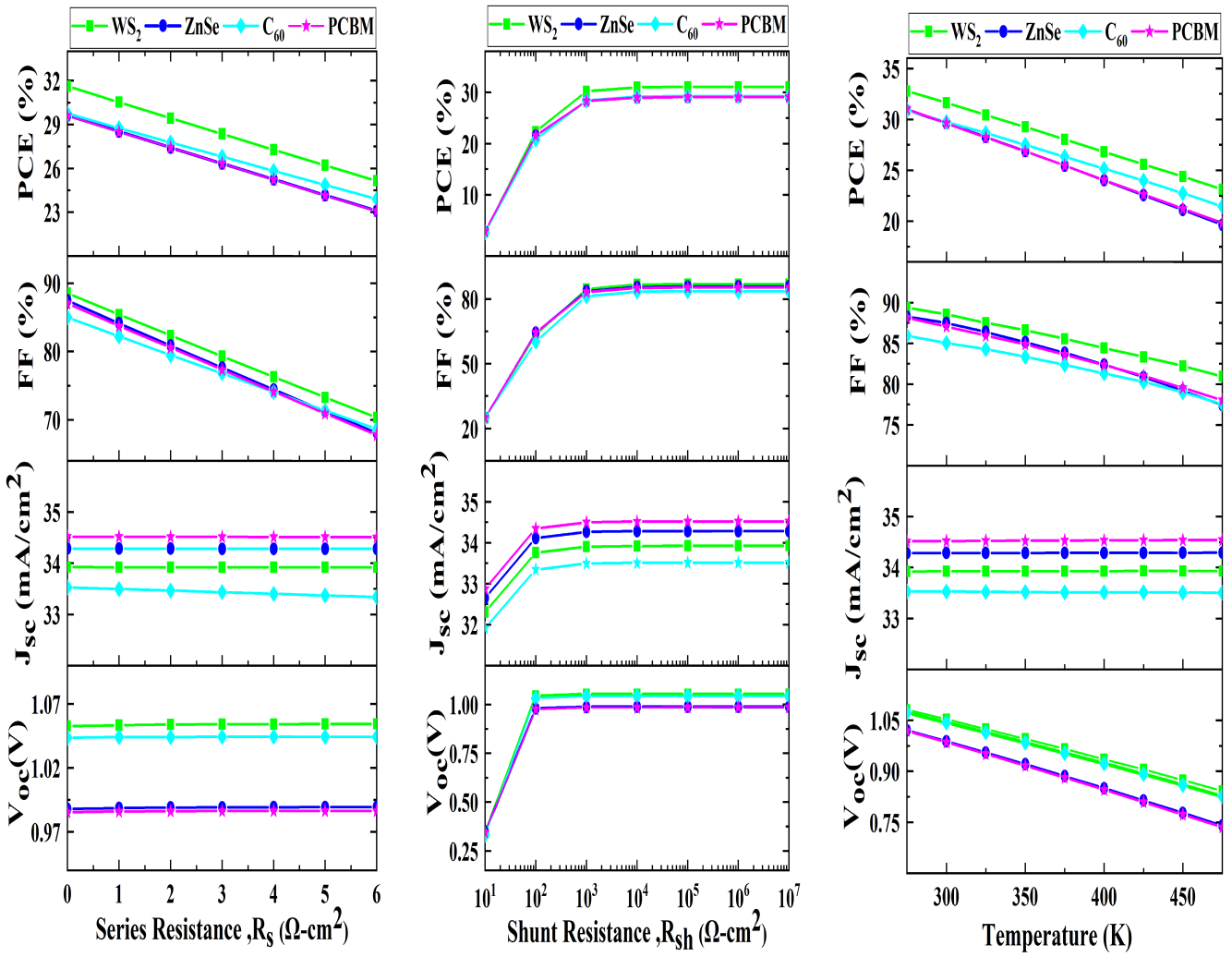

FIGURE 11. Impact of (a) series resistance (R_s), (b) shunt resistance (R_{sh}), and (c) temperature on Cell Performance.

is ranged from 0 Ω-cm^2 to 6 Ω-cm^2. It has been observed that the FF and PCE have decreased by an average of 20% from their maximum value due to increasing power dissipation for all four perovskite device structures [73]. The lowest PCE and FF values were shown by PCBM ETL-based structure, whilst the highest PCE and FF values were shown by WS_2 ETL-based structure for the variation of R_s. The V_{OC} and J_{SC} remained almost unchanged with increasing series resistance for all configurations. That means the variation in series resistance can't influence the V_{OC} as well as J_{SC} for the investigated device configurations. A similar pattern of results where series resistance had no impact on the current was reported by Sunny et al. [74]. Another study by Pooja et al. reported that series resistance could not alter the open circuit voltage [75]. However, it can be stated that series resistance needs to be minimized to a minimum value so that the best performance can be attained.

2) IMPACT OF SHUNT RESISTANCE (R_{SH})

Shunt resistance is a parallel resistance that allows current to bypass the absorbing layer and decreases efficiency due to fabrication defects [72]. Figure 11(b) shows the impact of R_{sh} on the key parameters of WS_2, ZnSe, C_{60} and PCBM-based PSC. R_{sh} was varied from 10^1 Ω-cm^2 to 10^7 Ω-cm^2 and the Series Resistance (R_s) was kept fixed at 0.5 Ω-cm^2. The values of performance parameters followed the same trend as R_{sh} is increased. From 10^1 Ω-cm^2, all the parameters started to enhance decisively. This trend continued till 10^3 Ω-cm^2. After that, they hold the same value though R_{sh} increases. It can be observed from the figure that, SC with WS_2 ETL exhibits the highest PCE, while the SC with PCBM ETL demonstrates the lowest PCE value within the specified range. Lower R_{sh} creates the alternating path for the photogenerated current which results in output power loss [76]. So, higher R_{sh} is better for device performance.

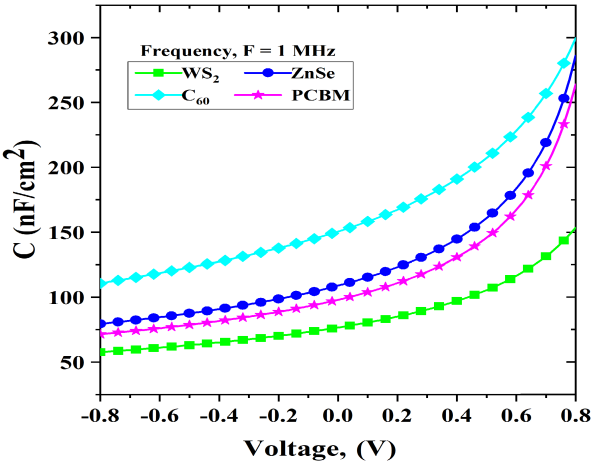

FIGURE 12. Capacitance vs voltage curve.

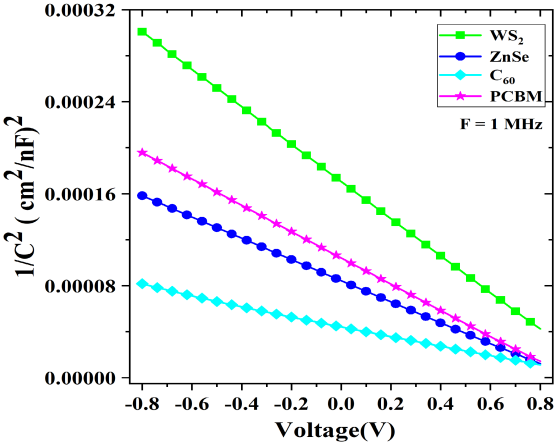

FIGURE 13. Mott–Schottky ($1/C^2$) lines vs voltage curve.

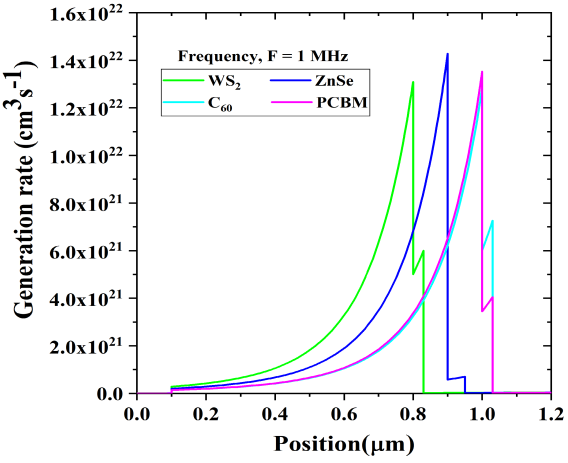

FIGURE 14. Generation rate curve for four PSCs.

3) IMPACT OF TEMPERATURE

To observe the impact of the environment in PSC, the temperature is ranged between 275 K to 450 K. Figure 11(c) demonstrates the effect of temperature on cell parameters. The simulation found that for all structures, a rise in temperature resulted in a drop in the V_{OC}, FF, and PCE, while the J_{SC} almost remained constant. The V_{OC} value has reduced as the temperature is increased due to its inverse relationship with the saturation current density [5]. A similar downtrend can be observed in the case of FF as well as PCE for all structures. The rise in temperature causes an improvement in series resistance, which in turn reduces the FF as well as the efficiency of the device [77], [78]. The pattern of the constant behavior of current throughout the rise in temperature was reported by Sunny et al. [74].

G. EFFECT OF CAPACITANCE AND MOTT-SCHOTTKY LINES

Figure 12 and Figure 13 illustrates the impact of capacitance along with M-S with the voltage variation from -0.8 volt to +0.8 volt for four individual configurations. The simulation had been performed at a higher frequency of 1 MHz to exclude the effect of traps situated internally at a deep level [79]. In Figure 12, an increment in supply voltage causes the capacitance to rise exponentially. As there are several junctions, the plots are curved and not linear in characteristics. The C_{60} ETL-based structure had the highest capacitance, while the WS_2 ETL had the lowest at 0.8 V. It can be assumed that when the bias is off, the device is in the depletion region. When the depletion width is nearly the same as the thickness of the absorber, the forward bias induces the capacitance to increase considerably [80]. The capacitance decreases significantly when a reverse bias is applied because the saturation current increases [81]. On the other side, the diffusion potential (V_{bi}) is observed from the Mott- Schottky plot. The slope between $1/C^2$ and V curve represents the defect density [82]. The MS values decreased for every structure in this work with rising voltage, which is consistent with previous research study [79].

H. EFFECT OF GENERATION RATE AND RECOMBINATION RATE

Electron-hole pairs are formed when an electron is stimulated from the valence band towards the conduction band, creating a hole [83]. Figure 14 shows that WS_2, C_{60}, ZnSe, and PCBM-based structures had a greater rate of generation at depths of 0.8 μm, 1 μm, 0.9 μm, and 1 μm, respectively. The recombination rate inversely combines and annihilates the generated electrons and holes [84]. According to Figure 15, the recombination has taken place in the 0.1μm - 1μm range. The recombination rate distribution is not uniform due to the presence of grain boundaries and defects in different layers [85]. However, the structures demonstrated significant recombination occur at 0.1 μm and 0.9 μm. The depth of 0.1 μm represents the HTL/Absorber interface and the depth of 0.9 μm represents the Absorber/ETL interface. Recombination tends to be more apparent at interfaces due to energy level mismatch, defect or trap States. The differences in energy levels between different materials at interfaces can result in increased carrier recombination. Furthermore, interfaces frequently possess defects or trap states which can function as recombination centers, facilitating electron and hole recombination [86].

TABLE 3. Comparison of PV parameters of $CsSnI_3$ based PSC with existing research work.

PSC Device	V_{OC} (V)	J_{SC} (mA/cm^2)	FF (%)	PCE (%)	References
FTO/WS_2/$CsSnI_3$/P3HT/Au	1.053	33.92	88.57	31.63	This work
FTO/ZnSe/$CsSnI_3$/P3HT/Au	0.988	34.28	87.50	29.64	This work
FTO/C_{60}/$CsSnI_3$/P3HT/Au	1.043	33.53	85.04	29.75	This work
FTO/PCBM/$CsSnI_3$/P3HT/Au	0.985	34.52	87.07	29.62	This work
CuS/$CsSnI_3$/TiO_2/ITO	0.99	33.5	86.6	28.76	[20]
FTO/TiO_2/$CsSnI_3$/Spiro-MeOTAD/Au	0.967	29.673	70.2	20.13	[17]
ITO/PCBM/$CsSnI_3$/CFTS/Se	0.87	33.99	83.46	24.73	[19]
FTO/TiO_2/$CsSnI_3$/P3HT/Au	0.972	34.70	78.21	26.40	[88]

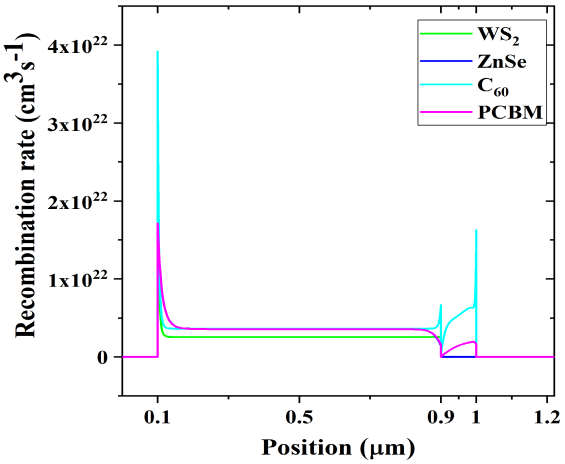

FIGURE 15. Recombination rate for four PSCs.

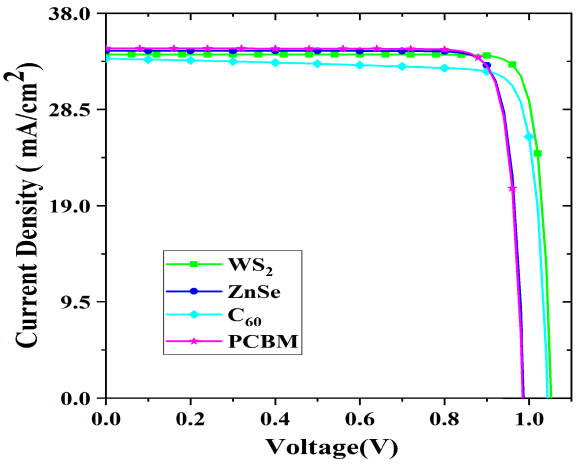

FIGURE 16. J–V characteristic curve for all four optimized designs.

I. J-V AND QE CHARACTERISTICS

Under a 1.5 AM lighting condition (100mW/cm^2), the J-V characteristics of the four configurations are shown in Figure 16. It was discovered that C_{60} ETL has shown the worst J-V characteristics compared to WS_2, ZnSe and PCBM. Despite its high V_{OC}, C_{60} ETL-associated PSC has a current density of 33.3 mA/cm^2. The value of current density was around 34.5 mA/cm^2 in PCBM and ZnSe despite the V_{OC} being less than 1.0 V. Meanwhile, the value of the current density in WS_2 was 33.92 mA/cm^2. Figure 17 displays the wavelength-quantum efficiency (QE) relationship for these structures. A similar pattern is found for all the structures. It is observed that at wavelengths between the 0.36 μm and 0.6 μm, QE for WS_2, ZnSe, and PCBM is almost 100%, whereas C_{60} showed the worst QE (90%) and it rises to 100% beyond 0.7μm wavelength. Solar cells having QE 100% means that it has absorbed almost incident photons in order to create electron-hole pairs and minimize all the recombination [87]. Furthermore, beyond this wavelength range, photons with higher wavelengths cause lower QE. This is due to the inability of those photons to generate high enough energy to create electron-hole pairs. Finally, the quantum efficiency falls to zero at the wavelength of 0.96 μm. Therefore, the configurations mostly cover the visible light spectrum.

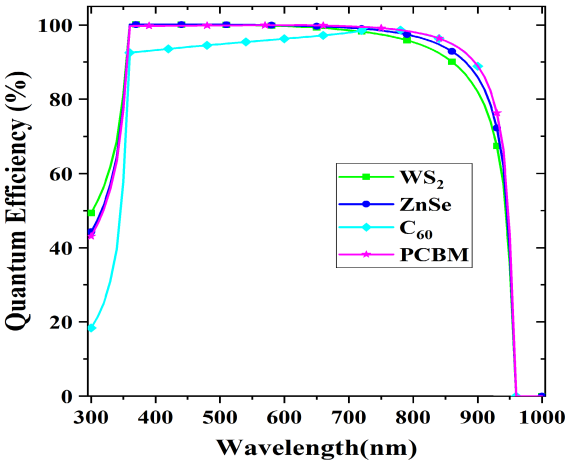

FIGURE 17. Quantum efficiency curve for all four optimized designs.

J. OPTIMIZED STRUCTURE

Different ETL materials were incorporated into the device structure using P3HT as the HTL and the parameters such as the thickness, doping level, defect density of different layers,temperature, parasitic resistance etc. are optimized.

Among the several ETL candidates implemented, including WS_2, ZnSe, C_{60}, and PCBM, it's evident that WS_2 can be recognized as a potential and efficient ETL material for lead-free Sn-based perovskite solar cells with an improved V_{OC} of 1.053 V, the device architecture demonstrated an efficiency of 31.63% that is comparable to previously reported studies mentioned in Table 3.

IV. CONCLUSION

In this study, a highly efficient, lead-free, and sustainable PSC based on $CsSnI_3$ has been recommended with a new combination of FTO/WS_2/$CsSnI_3$/P3HT/Au by evaluating the impacts of various ETL materials on device performance and improving various solar cell parameters along with the operating conditions of the solar cell. Additionally, the performance is compared against previously published literature. The proposed structure features a FF of 88.57%, a short circuit current density of 33.92 mA/cm^2, an efficiency of 31.63% and an open-circuit voltage of 1.053V. The structure also exhibits excellent quantum efficiency in the near IR and visible spectrum. Hopefully, in the future, this research will aid in the development of lead-free solar cells that are more stable and can serve as a foundation for flexible technology.

ACKNOWLEDGMENT

The authors would like to acknowledge Prof. Marc Burgelman of the University of Gent, Belgium, for generously providing the required SCAPS-1D software. The availability of this software considerably enriched research efforts and broadened the range of analytical capabilities.

REFERENCES

[1] F. Barbir, T. N. Veziroglu, and H. J. Plass, "Environmental damage due to fossil fuels use," *Int. J. Hydrogen Energy*, vol. 15, no. 10, 1990, Art. no. 739749, doi: 10.1016/0360-3199(90)90005J.

[2] S. Shafiee and E. Topal, "When will fossil fuel reserves be diminished?" *Energy Policy*, vol. 37, no. 1, pp. 181–189, Jan. 2009, doi: 10.1016/j.enpol.2008.08.016.

[3] J. P. A. Jebakumar, D. J. Moni, D. Gracia, and M. D. Shallet, "Design and simulation of inorganic perovskite solar cell," *Appl. Nanosci.*, vol. 12, no. 5, pp. 1507–1518, May 2022, doi: 10.1007/s13204-021-02268-7.

[4] M. R. Islam, K. Sumathy, and S. U. Khan, "Solar water heating systems and their market trends," *Renew. Sustain. Energy Rev.*, vol. 17, pp. 1–25, Jan. 2013, doi: 10.1016/j.rser.2012.09.011.

[5] K. Yoshikawa, H. Kawasaki, W. Yoshida, T. Irie, K. Konishi, K. Nakano, T. Uto, D. Adachi, M. Kanematsu, H. Uzu, and K. Yamamoto, "Silicon heterojunction solar cell with interdigitated back contacts for a photoconversion efficiency over 26%," *Nature Energy*, vol. 2, no. 5, Mar. 2017, Art. no. 17032, doi: 10.1038/nenergy.2017.32.

[6] Z. Song, C. L. McElvany, A. B. Phillips, I. Celik, P. W. Krantz, S. C. Watthage, G. K. Liyanage, D. Apul, and M. J. Heben, "A technoeconomic analysis of perovskite solar module manufacturing with low-cost materials and techniques," *Energy Environ. Sci.*, vol. 10, no. 6, pp. 1297–1305, 2017, doi: 10.1039/C7EE00757D.

[7] A. Kojima, K. Teshima, Y. Shirai, and T. Miyasaka, "Organometal halide perovskites as visible-light sensitizers for photovoltaic cells," *J. Amer. Chem. Soc.*, vol. 131, no. 17, pp. 6050–6051, May 2009, doi: 10.1021/ja809598r.

[8] S.-P. Feng et al., "Roadmap on commercialization of metal halide perovskite photovoltaics," *J. Phys., Mater.*, vol. 6, no. 3, Jun. 2023, Art. no. 032501, doi: 10.1088/2515-7639/acc893.

[9] T. Krishnamoorthy, H. Ding, C. Yan, W. L. Leong, T. Baikie, Z. Zhang, M. Sherburne, S. Li, M. Asta, N. Mathews, and S. G. Mhaisalkar, "Lead-free germanium iodide perovskite materials for photovoltaic applications," *J. Mater. Chem. A*, vol. 3, no. 47, pp. 23829–23832, 2015, doi: 10.1039/C5TA05741H.

[10] G. Wang, J. Chang, J. Bi, M. Lei, C. Wang, and Q. Qiao, "Inorganic $CsSnI_3$ perovskite solar cells: The progress and future prospects," *Sol. RRL*, vol. 6, no. 4, Apr. 2022, Art. no. 2100841, doi: 10.1002/solr.202100841.

[11] Z. Chen, J. J. Wang, Y. Ren, C. Yu, and K. Shum, "Schottky solar cells based on $CsSnI_3$ thin-films," *Appl. Phys. Lett.*, vol. 101, no. 9, Aug. 2012, Art. no. 093901, doi: 10.1063/1.4748888.

[12] Y. Wang, J. Tu, T. Li, C. Tao, X. Deng, and Z. Li, "Convenient preparation of $CsSnI_3$ quantum dots, excellent stability, and the highest performance of lead-free inorganic perovskite solar cells so far," *J. Mater. Chem. A*, vol. 7, no. 13, pp. 7683–7690, 2019, doi: 10.1039/C8TA10901J.

[13] S. Ma, X. Gu, A. K. Kyaw, D. H. Wang, S. Priya, and T. Ye, "Fully inorganic $CsSnI_3$-based solar cells with >6% efficiency and enhanced stability enabled by mixed electron transport layer," *ACS Appl. Mater. Interface*, vol. 13, no. 1, pp. 1345–1352, Jan. 2021, doi: 10.1021/acsami.0c16634.

[14] H. Ban, T. Nakajima, Z. Liu, H. Yu, Q. Sun, L. Dai, Y. Shen, X.-L. Zhang, J. Zhu, P. Chen, and M. Wang, "Over 8% efficient $CsSnI_3$-based mesoporous perovskite solar cells enabled by two-step thermal annealing and surface cationic coordination dual treatment," *J. Mater. Chem. A*, vol. 10, no. 7, pp. 3642–3649, 2022, doi: 10.1039/D1TA09811J.

[15] T. Ye, X. Wang, K. Wang, S. Ma, D. Yang, Y. Hou, J. Yoon, K. Wang, and S. Priya, "Localized electron density engineering for stabilized B-γ $CsSnI_3$-based perovskite solar cells with efficiencies >10%," *ACS Energy Lett.*, vol. 6, pp. 1480–1489, Mar. 2021, doi: 10.1021/acsenergylett.1c00342.

[16] L.-J. Chen, C.-R. Lee, Y.-J. Chuang, Z.-H. Wu, and C. Chen, "Synthesis and optical properties of lead-free cesium tin halide perovskite quantum rods with high-performance solar cell application," *J. Phys. Chem. Lett.*, vol. 7, no. 24, pp. 5028–5035, Dec. 2016, doi: 10.1021/acs.jpclett.6b02344.

[17] S. Lin, B. Zhang, T.-Y. Lü, J.-C. Zheng, H. Pan, H. Chen, C. Lin, X. Li, and J. Zhou, "Inorganic lead-free B-γ-$CsSnI_3$ perovskite solar cells using diverse electron-transporting materials: A simulation study," *ACS Omega*, vol. 6, no. 40, pp. 26689–26698, Oct. 2021, doi: 10.1021/acsomega.1c04096.

[18] B. Wu, Y. Zhou, G. Xing, Q. Xu, H. F. Garces, A. Solanki, T. W. Goh, N. P. Padture, and T. C. Sum, "Long minority-carrier diffusion length and low surface-recombination velocity in inorganic lead-free $CsSnI_3$ perovskite crystal for solar cells," *Adv. Funct. Mater.*, vol. 27, no. 7, Feb. 2017, Art. no. 1604818, doi: 10.1002/adfm.201604818.

[19] M. K. Hossain, M. S. Uddin, G. F. I. Toki, M. K. A. Mohammed, R. Pandey, J. Madan, M. F. Rahman, M. R. Islam, S. Bhattarai, H. Bencherif, D. P. Samajdar, M. Amami, and D. K. Dwivedi, "Achieving above 24% efficiency with non-toxic $CsSnI_3$ perovskite solar cells by harnessing the potential of the absorber and charge transport layers," *RSC Adv.*, vol. 13, no. 34, pp. 23514–23537, 2023, doi: 10.1039/D3RA02910G.

[20] A. Hosen, S. Rahman, M. Brella, and S. R. A. Ahmed, "Impact of hole transport layers in inorganic lead-free B-γ-$CsSnI_3$ perovskite solar cells: A numerical analysis," in *Proc. ECP*, May 2022, p. 41, doi: 10.3390/ECP2022-12611.

[21] P. Zhou, T. Bu, S. Shi, L. Li, Y. Zhang, Z. Ku, Y. Peng, J. Zhong, Y.-B. Cheng, and F. Huang, "Efficient and stable mixed perovskite solar cells using P3HT as a hole transporting layer," *J. Mater. Chem. C*, vol. 6, no. 21, pp. 5733–5737, 2018, doi: 10.1039/C8TC01345D.

[22] M. Neophytou, M. De Bastiani, N. Gasparini, E. Aydin, E. Ugur, A. Seitkhan, F. Moruzzi, Y. Choaie, A. J. Ramadan, J. R. Troughton, R. Hallani, A. Savva, L. Tsetseris, S. Inal, D. Baran, F. Laquai, T. D. Anthopoulos, H. J. Snaith, S. De Wolf, and I. McCulloch, "Enhancing the charge extraction and stability of perovskite solar cells using strontium titanate ($SrTiO_3$) electron transport layer," *ACS Appl. Energy Mater.*, vol. 2, no. 11, pp. 8090–8097, Nov. 2019, doi: 10.1021/acsaem.9b01567.

[23] E. Karimi and S. M. B. Ghorashi, "Investigation of the influence of different hole-transporting materials on the performance of perovskite solar cells," *Optik*, vol. 130, pp. 650–658, Feb. 2017, doi: 10.1016/j.ijleo.2016.10.122.

[24] H.-J. Du, W.-C. Wang, and J.-Z. Zhu, "Device simulation of lead-free $CH_3NH_3SnI_3$ perovskite solar cells with high efficiency," *Chin. Phys. B*, vol. 25, no. 10, Oct. 2016, Art. no. 108802, doi: 10.1088/1674-1056/25/10/108802.

[25] J. C. Nolasco, R. Cabré, J. Ferré-Borrull, L. F. Marsal, M. Estrada, and J. Pallarès, "Extraction of poly (3-hexylthiophene) (P3HT) properties from dark current voltage characteristics in a P3HT/n-crystalline-silicon solar cell," *J. Appl. Phys.*, vol. 107, no. 4, p. 44505, Feb. 2010, doi: 10.1063/1.3296294.

[26] Y. Raoui, H. Ez-Zahraouy, N. Tahiri, O. El Bounagui, S. Ahmad, and S. Kazim, "Performance analysis of $MAPbI_3$ based perovskite solar cells employing diverse charge selective contacts: Simulation study," *Sol. Energy*, vol. 193, pp. 948–955, Nov. 2019, doi: 10.1016/j.solener.2019.10.009.

[27] S. Lin, "Inorganic lead-free β-γ-$CsSnI_3$ perovskite solar cells using diverse electron-transporting materials: A simulation study," *ACS Omega*, vol. 6, no. 40, pp. 26689–26698, Jul. 2021, doi: 10.1021/acsomega.1c04096.

[28] N. Singh, A. Agarwal, and M. Agarwal, "Performance evaluation of lead–free double-perovskite solar cell," *Opt. Mater.*, vol. 114, Apr. 2021, Art. no. 110964, doi: 10.1016/j.optmat.2021.110964.

[29] S. Abdelaziz, A. Zekry, A. Shaker, and M. Abouelatta, "Investigating the performance of formamidinium tin-based perovskite solar cell by SCAPS device simulation," *Opt. Mater.*, vol. 101, Mar. 2020, Art. no. 109738, doi: 10.1016/j.optmat.2020.109738.

[30] K. Sobayel, M. Akhtaruzzaman, K. S. Rahman, M. T. Ferdaous, Z. A. Al-Mutairi, H. F. Alharbi, N. H. Alharthi, M. R. Karim, S. Hasmady, and N. Amin, "A comprehensive defect study of tungsten disulfide (WS_2) as electron transport layer in perovskite solar cells by numerical simulation," *Results Phys.*, vol. 12, pp. 1097–1103, Mar. 2019, doi: 10.1016/j.rinp.2018.12.049.

[31] A. P. Samantilleke, M. H. Boyle, J. Young, and I. M. Dharmadasa, "Growth of n-type and p-type ZnSe thin films using an electrochemical technique for applications in large area optoelectronic devices," *J. Mater. Sci. Mater. Electron.*, vol. 9, no. 3, pp. 231–235, 1998, doi: 10.1023/A:1008886410204.

[32] J. Hossain, "Design and simulation of double-heterojunction solar cells based on Si and GaAs wafers," *J. Phys. Commun.*, vol. 5, no. 8, Aug. 2021, Art. no. 085008, doi: 10.1088/2399-6528/ac1bc0.

[33] Y. Gan, X. Bi, Y. Liu, B. Qin, Q. Li, Q. Jiang, and P. Mo, "Numerical investigation energy conversion performance of tin-based perovskite solar cells using cell capacitance simulator," *Energies*, vol. 13, no. 22, p. 5907, Nov. 2020, doi: 10.3390/en13225907.

[34] M. K. Hossain, M. K. A. Mohammed, R. Pandey, A. A. Arnab, M. H. K. Rubel, K. M. Hossain, M. H. Ali, M. F. Rahman, H. Bencherif, J. Madan, M. R. Islam, D. P. Samajdar, and S. Bhattarai, "Numerical analysis in DFT and SCAPS-1D on the influence of different charge transport layers of $CsPbBr_3$ perovskite solar cells," *Energy Fuels*, vol. 37, no. 8, pp. 6078–6098, Apr. 2023, doi: 10.1021/acs.energyfuels.3c00035.

[35] M. S. S. Basyoni, M. M. Salah, M. Mousa, A. Shaker, A. Zekry, M. Abouelatta, M. T. Alshammari, K. A. Al-Dhlan, and C. Gontrand, "On the investigation of interface defects of solar cells: Lead-based vs lead-free perovskite," *IEEE Access*, vol. 9, pp. 130221–130232, 2021, doi: 10.1109/ACCESS.2021.3114383.

[36] Y. He, L. Xu, C. Yang, X. Guo, and S. Li, "Design and numerical investigation of a lead-free inorganic layered double perovskite $Cs_4CuSb_2Cl_{12}$ nanocrystal solar cell by SCAPS-1D," *Nanomaterials*, vol. 11, no. 9, p. 2321, Sep. 2021, doi: 10.3390/nano11092321.

[37] M. Burgelman, P. Nollet, and S. Degrave, "Modelling polycrystalline semiconductor solar cells," *Thin Solid Films*, vols. 361–362, pp. 527–532, Feb. 2000, doi: 10.1016/S0040-6090(99)00825-1.

[38] S. S. Hussain, S. Riaz, G. A. Nowsherwan, K. Jahangir, A. Raza, M. J. Iqbal, I. Sadiq, S. M. Hussain, and S. Naseem, "Numerical modeling and optimization of lead-free hybrid double perovskite solar cell by using SCAPS-1D," *J. Renew. Energy*, vol. 2021, pp. 1–12, Jul. 2021, doi: 10.1155/2021/6668687.

[39] F. Liu, J. Zhu, J. Wei, Y. Li, M. Lv, S. Yang, B. Zhang, J. Yao, and S. Dai, "Numerical simulation: Toward the design of high-efficiency planar perovskite solar cells," *Appl. Phys. Lett.*, vol. 104, no. 25, Jun. 2014, Art. no. 253508, doi: 10.1063/1.4885367.

[40] S. Ahmed, F. Jannat, M. A. K. Khan, and M. A. Alim, "Numerical development of eco-friendly Cs_2TiBr_6 based perovskite solar cell with all-inorganic charge transport materials via SCAPS-1D," *Optik*, vol. 225, Jan. 2021, Art. no. 165765, doi: 10.1016/j.ijleo.2020.165765.

[41] F. Anwar, R. Mahbub, S. S. Satter, and S. M. Ullah, "Effect of different HTM layers and electrical parameters on ZnO nanorod-based lead-free perovskite solar cell for high-efficiency performance," *Int. J. Photoenergy*, vol. 2017, pp. 1–9, Nov. 2017, doi: 10.1155/2017/9846310.

[42] P. Roy, N. K. Sinha, S. Tiwari, and A. Khare, "Influence of defect density and layer thickness of absorption layer on the performance of tin based perovskite solar cell," *IOP Conf. Ser., Mater. Sci. Eng.*, vol. 798, no. 1, Mar. 2020, Art. no. 012020, doi: 10.1088/1757-899x/798/1/012020.

[43] H. Nazem, H. P. Dizaj, and N. E. Gorji, "Modeling of Jsc and Voc versus the grain size in CdTe, CZTS and perovskite thin film solar cells," *Superlattices Microstructures*, vol. 128, pp. 421–427, Apr. 2019, doi: 10.1016/j.spmi.2019.02.002.

[44] N. Lakhdar and A. Hima, "Electron transport material effect on performance of perovskite solar cells based on $CH_3NH_3GeI_3$," *Opt. Mater.*, vol. 99, Jan. 2020, Art. no. 109517, doi: 10.1016/j.optmat.2019.109517.

[45] V. Garg, A. Kumar, and P. Sharma, "Numerical simulation of novel lead-free $Cs_3Sb_2Br_9$ absorber-based highly efficient perovskite solar cell," *Opt. Mater.*, vol. 122, Dec. 2021, Art. no. 111715, doi: 10.1016/j.optmat.2021.111715.

[46] E. S. Hossain, P. Chelvanathan, S. A. Shahahmadi, K. Sopian, B. Bais, and N. Amin, "Performance assessment of Cu_2SnS_3 (CTS) based thin film solar cells by AMPS-1D," *Current Appl. Phys.*, vol. 18, no. 1, pp. 79–89, Jan. 2018, doi: 10.1016/j.cap.2017.10.009.

[47] A. Maiti, S. Chatterjee, L. Peedikakkandy, and A. J. Pal, "Defects and their passivation in hybrid halide perovskites toward solar cell applications," *Sol. RRL*, vol. 4, no. 12, Nov. 2020, Art. no. 2000505, doi: 10.1002/solr.202000505.

[48] M. S. Chowdhury, S. A. Shahahmadi, P. Chelvanathan, S. K. Tiong, N. Amin, K. Techato, N. Nuthammachot, T. Chowdhury, and M. Suklueng, "Effect of deep-level defect density of the absorber layer and n/i interface in perovskite solar cells by SCAPS-1D," *Results Phys.*, vol. 16, Mar. 2020, Art. no. 102839, doi: 10.1016/j.rinp.2019.102839.

[49] A. Raj, M. Kumar, H. Bherwani, A. Gupta, and A. Anshul, "Evidence of improved power conversion efficiency in lead-free $CsGeI_3$ based perovskite solar cell heterostructure via scaps simulation," *J. Vac. Sci. Technol. B, Nanotechnol. Microelectron., Mater., Process., Meas., Phenomena*, vol. 39, no. 1, Jan. 2021, Art. no. 012401, doi: 10.1116/6.0000718.

[50] S. A. Moiz, A. N. M. Alahmadi, and A. J. Aljohani, "Design of a novel lead-free perovskite solar cell for 17.83% efficiency," *IEEE Access*, vol. 9, pp. 54254–54263, 2021, doi: 10.1109/ACCESS.2021.3070112.

[51] K. Shivesh, I. Alam, A. K. Kushwaha, M. Kumar, and S. V. Singh, "Investigating the theoretical performance of Cs_2TiBr_6-based perovskite solar cell with La-doped $BaSnO_3$ and $CuSbS_2$ as the charge transport layers," *Int. J. Energy Res.*, vol. 46, no. 5, pp. 6045–6064, Apr. 2022, doi: 10.1002/er.7546.

[52] M. N. H. Riyad, A. Sunny, M. M. Khatun, S. Rahman, and S. R. A. Ahmed, "Performance evaluation of WS_2 as buffer and $Sb2S_3$ as hole transport layer in CZTS solar cell by numerical simulation," *Eng. Rep.*, vol. 5, no. 5, Nov. 2022, Art. no. e12600, doi: 10.1002/eng2.12600.

[53] M. J. Nayeen, B. K. Mondal, S. R. Basu, and J. Hossain, "Theoretical exploration of high V_{OC} in Cu_2SnS_3 thin film solar cells towards high efficiency," *Sol. Energy*, vol. 265, Nov. 2023, Art. no. 112076, doi: 10.1016/j.solener.2023.112076.

[54] S. Z. Haider, H. Anwar, and M. Wang, "A comprehensive device modelling of perovskite solar cell with inorganic copper iodide as hole transport material," *Semicond. Sci. Technol.*, vol. 33, no. 3, Mar. 2018, Art. no. 035001, doi: 10.1088/1361-6641/aaa596.

[55] D. Prochowicz, M. M. Tavakoli, M. Wolska-Pietkiewicz, M. Jędrzejewska, S. Trivedi, M. Kumar, S. M. Zakeeruddin, J. Lewiński, M. Graetzel, and P. Yadav, "Suppressing recombination in perovskite solar cells via surface engineering of TiO_2 ETL," *Sol. Energy*, vol. 197, pp. 50–57, Feb. 2020, doi: 10.1016/j.solener.2019.12.070.

[56] D. K. Sarkar, A. K. M. Hasan, M. Mottakin, V. Selvanathan, K. Sobayel, M. Ariful Islam, G. Muhammad, M. Aminuzzaman, M. Shahiduzzaman, K. Sopian, and M. Akhtaruzzaman, "Lead free efficient perovskite solar cell device optimization and defect study using Mg doped $CuCrO_2$ as HTL and WO_3 as ETL," *Sol. Energy*, vol. 243, pp. 215–224, Sep. 2022, doi: 10.1016/j.solener.2022.07.013.

[57] G. Pindolia, S. M. Shinde, and P. K. Jha, "Optimization of an inorganic lead free $RbGeI_3$ based perovskite solar cell by SCAPS-1D simulation," *Sol. Energy*, vol. 236, pp. 802–821, Apr. 2022, doi: 10.1016/j.solener.2022.03.053.

[58] N. Rai, S. Rai, P. K. Singh, P. Lohia, and D. K. Dwivedi, "Analysis of various ETL materials for an efficient perovskite solar cell by numerical simulation," *J. Mater. Sci., Mater. Electron.*, vol. 31, no. 19, pp. 16269–16280, Oct. 2020, doi: 10.1007/s10854-020-04175-z.

[59] M. Yue, J. Su, P. Zhao, Z. Lin, J. Zhang, J. Chang, and Y. Hao, "Optimizing the performance of $CsPbI_3$-based perovskite solar cells via doping a ZnO electron transport layer coupled with interface engineering," *Nano-Micro Lett.*, vol. 11, no. 1, p. 91, Dec. 2019, doi: 10.1007/s40820-019-0320-y.

[60] K. Lim, S. Ahn, H. Kim, M. Choi, D. H. Huh, and T. Lee, "Self-doped conducting polymer as a hole-extraction layer in organic–inorganic hybrid perovskite solar cells," *Adv. Mater. Interface*, vol. 3, no. 9, May 2016, Art. no. 1500678, doi: 10.1002/admi.201500678.

[61] M. K. Hossain, G. F. I. Toki, I. Alam, R. Pandey, D. P. Samajdar, M. F. Rahman, M. R. Islam, M. H. K. Rubel, H. Bencherif, J. Madan, and M. K. A. Mohammed, "Numerical simulation and optimization of a $CsPbI_3$-based perovskite solar cell to enhance the power conversion efficiency," *New J. Chem.*, vol. 47, no. 10, pp. 4801–4817, 2023, doi: 10.1039/D2NJ06206B.

[62] U. Mandadapu, "Simulation and analysis of lead based perovskite solar cell using SCAPS-1D," *Indian J. Sci. Technol.*, vol. 10, no. 1, pp. 1–8, Jan. 2017, doi: 10.17485/ijst/2017/v11i10/110721.

[63] M. K. Hossain, G. F. I. Toki, J. Madan, R. Pandey, H. Bencherif, M. K. A. Mohammed, M. R. Islam, M. H. K. Rubel, M. F. Rahman, S. Bhattarai, and D. P. Samajdar, "A comprehensive study of the optimization and comparison of cesium halide perovskite solar cells using ZnO and Cu_2FeSnS_4 as charge transport layers," *New J. Chem.*, vol. 47, no. 18, pp. 8602–8624, 2023, doi: 10.1039/D3NJ00320E.

[64] O. Ahmad, A. Rashid, M. W. Ahmed, M. F. Nasir, and I. Qasim, "Performance evaluation of Au/p-CdTe/Cs_2TiI_6/n-TiO_2/ITO solar cell using SCAPS-1D," *Opt. Mater.*, vol. 117, Jul. 2021, Art. no. 111105, doi: 10.1016/j.optmat.2021.111105.

[65] S. Shao and M. A. Loi, "The role of the interfaces in perovskite solar cells," *Adv. Mater. Interface*, vol. 7, no. 1, Jan. 2020, Art. no. 1901469, doi: 10.1002/admi.201901469.

[66] M. K. Hossain, D. P. Samajdar, R. C. Das, A. A. Arnab, M. F. Rahman, M. H. K. Rubel, M. R. Islam, H. Bencherif, R. Pandey, J. Madan, and M. K. A. Mohammed, "Design and simulation of Cs_2BiAgI_6 double perovskite solar cells with different electron transport layers for efficiency enhancement," *Energy Fuels*, vol. 37, no. 5, pp. 3957–3979, Feb. 2023, doi: 10.1021/acs.energyfuels.3c00181.

[67] Y. H. Khattak, F. Baig, H. Toura, S. Beg, and B. M. Soucase, "CZTSe kesterite as an alternative hole transport layer for $MASnI_3$ perovskite solar cells," *J. Electron. Mater.*, vol. 48, no. 9, pp. 5723–5733, Sep. 2019, doi: 10.1007/s11664-019-07374-5.

[68] C. M. Wolff, P. Caprioglio, M. Stolterfoht, and D. Neher, "Non-radiative recombination in perovskite solar cells: The role of interfaces," *Adv. Mater.*, vol. 31, no. 52, Dec. 2019, Art. no. 1902762, doi: 10.1002/adma.201902762.

[69] T. Minemoto and M. Murata, "Device modeling of perovskite solar cells based on structural similarity with thin film inorganic semiconductor solar cells," *J. Appl. Phys.*, vol. 116, no. 5, Aug. 2014, Art. no. 054505, doi: 10.1063/1.4891982.

[70] K. Tan, P. Lin, G. Wang, Y. Liu, Z. Xu, and Y. Lin, "Controllable design of solid-state perovskite solar cells by SCAPS device simulation," *Solid-State Electron.*, vol. 126, pp. 75–80, Dec. 2016, doi: 10.1016/j.sse.2016.09.012.

[71] M. F. Rahman, M. M. A. Moon, M. K. Hossain, M. H. Ali, M. D. Haque, A. Kuddus, J. Hossain, and A. B. Md. Ismail, "Concurrent investigation of antimony chalcogenide (Sb_2Se_3 and Sb_2S_3)-based solar cells with a potential WS_2 electron transport layer," *Heliyon*, vol. 8, no. 12, Dec. 2022, Art. no. e12034, doi: 10.1016/j.heliyon.2022.e12034.

[72] S. Ahmmed, A. Aktar, J. Hossain, and A. B. M. Ismail, "Enhancing the open circuit voltage of the SnS based heterojunction solar cell using NiO HTL," *Sol. Energy*, vol. 207, pp. 693–702, Sep. 2020, doi: 10.1016/j.solener.2020.07.003.

[73] D. Jayan K, V. Sebastian, and J. Kurian, "Simulation and optimization studies on $CsPbI_3$ based inorganic perovskite solar cells," *Sol. Energy*, vol. 221, pp. 99–108, Jun. 2021, doi: 10.1016/j.solener.2021.04.030.

[74] A. Sunny, S. Rahman, M. M. Khatun, and S. R. A. Ahmed, "Numerical study of high performance HTL-free $CH_3NH_3SnI_3$-based perovskite solar cell by SCAPS-1D," *AIP Adv.*, vol. 11, no. 6, Jun. 2021, Art. no. 065102, doi: 10.1063/5.0049646.

[75] P. Tiwari, M. F. Alotaibi, Y. Al-Hadeethi, V. Srivastava, B. Arkook, S. Sadanand, P. Lohia, D. K. Dwivedi, A. Umar, H. Algadi, and S. Baskoutas, "Design and simulation of efficient SnS-based solar cell using spiro-OMeTAD as hole transport layer," *Nanomaterials*, vol. 12, no. 14, p. 2506, Jul. 2022, doi: 10.3390/nano12142506.

[76] J. Ding, X. Cheng, and T. Fu, "Analysis of series resistance and P–T characteristics of the solar cell," *Vacuum*, vol. 77, no. 2, pp. 163–167, Jan. 2005, doi: 10.1016/j.vacuum.2004.08.019.

[77] F. Behrouznejad, S. Shahbazi, N. Taghavinia, H.-P. Wu, and E. W.-G. Diau, "A study on utilizing different metals as the back contact of $CH_3NH_3PbI_3$ perovskite solar cells," *J. Mater. Chem. A*, vol. 4, no. 35, pp. 13488–13498, 2016, doi: 10.1039/C6TA05938D.

[78] S. R. Raga, E. M. Barea, and F. Fabregat-Santiago, "Analysis of the origin of open circuit voltage in dye solar cells," *J. Phys. Chem. Lett.*, vol. 3, no. 12, pp. 1629–1634, Jun. 2012, doi: 10.1021/jz3005464.

[79] S. R. Meher, L. Balakrishnan, and Z. C. Alex, "Analysis of Cu_2ZnSnS_4/CdS based photovoltaic cell: A numerical simulation approach," *Superlattices Microstructures*, vol. 100, pp. 703–722, Dec. 2016, doi: 10.1016/j.spmi.2016.10.028.

[80] M. K. Hossain, M. H. K. Rubel, G. F. I. Toki, I. Alam, M. F. Rahman, and H. Bencherif"Effect of various electron and hole transport layers on the performance of $CsPbI_3$-based perovskite solar cells: A numerical investigation in DFT, SCAPS-1D, and wxAMPS frameworks," *ACS Omega*, vol. 7, no. 47, pp. 43210–43230, Nov. 2022, doi: 10.1021/acsomega.2c05912.

[81] K. Decock, S. Khelifi, and M. Burgelman, "Modelling multivalent defects in thin film solar cells," *Thin Solid Films*, vol. 519, no. 21, pp. 7481–7484, Aug. 2011, doi: 10.1016/j.tsf.2010.12.039.

[82] N. Kumar, J. Rani, and R. Kurchania, "Advancement in $CsPbBr_3$ inorganic perovskite solar cells: Fabrication, efficiency and stability," *Sol. Energy*, vol. 221, pp. 197–205, Jun. 2021, doi: 10.1016/j.solener.2021.04.042.

[83] Z. Zhang and J. T. Yates, "Direct observation of surface-mediated electron-hole pair recombination in TiO_2(110)," *J. Phys. Chem. C*, vol. 114, no. 7, pp. 3098–3101, Feb. 2010, doi: 10.1021/jp910404e.

[84] S. C. Choo, "Carrier generation-recombination in the space-charge region of an asymmetrical p-n junction," *Solid. State. Electron.*, vol. 11, no. 11, pp. 1069–1077, Nov. 1968, doi: 10.1016/0038-1101(68)90129-9.

[85] K. K. Maurya and V. N. Singh, "Sb_2Se_3/CZTS dual absorber layer based solar cell with 36.32 % efficiency: A numerical simulation," *J. Sci., Adv. Mater. Devices*, vol. 7, no. 2, Jun. 2022, Art. no. 100445, doi: 10.1016/j.jsamd.2022.100445.

[86] V. P. H. Huy and C.-W. Bark, "Review on surface modification of SnO_2 electron transport layer for high-efficiency perovskite solar cells," *Appl. Sci.*, vol. 13, no. 19, p. 10715, Sep. 2023, doi: 10.3390/app131910715.

[87] S.-W. Lee, S. Kim, S. Bae, K. Cho, T. Chung, L. E. Mundt, S. Lee, S. Park, H. Park, M. C. Schubert, S. W. Glunz, Y. Ko, Y. Jun, Y. Kang, H.-S. Lee, and D. Kim, "UV degradation and recovery of perovskite solar cells," *Sci. Rep.*, vol. 6, no. 1, p. 38150, Dec. 2016, doi: 10.1038/srep38150.

[88] B. K. Ravidas, M. K. Roy, and D. P. Samajdar, "Investigation of photovoltaic performance of lead-free $CsSnI_3$-based perovskite solar cell with different hole transport layers: First principle calculations and SCAPS-1D analysis," *Sol. Energy*, vol. 249, pp. 163–173, Jan. 2023, doi: 10.1016/j.solener.2022.11.025.

MD. FERDOUS WAHID (Graduate Student Member, IEEE) received the B.Sc. (Engg.) degree in electronics and communication engineering from the Khulna University of Engineering and Technology (KUET), Khulna, Bangladesh, in 2012, where he is currently pursuing the M.Sc. (Engg.) degree in electronics and communication engineering. He is a Faculty Member with Hajee Mohammad Danesh Science and Technology University (HSTU), Dinajpur, Bangladesh. His research interests include renewable energy, solar cell design, and biomedical image analysis using machine learning and deep learning techniques.

MD. SHAHRIAR RAHMAN (Student Member, IEEE) was born in Chuadanga, Bangladesh. He is currently pursuing the B.Sc. degree in electrical and electronic engineering (EEE) with Hajee Mohammad Danesh Science and Technology University, Dinajpur, Bangladesh. He is involved in research in the area of renewable energy technology. His research interests include renewable and distributed generation, smart grids, and solar PV systems.

NOWSHAD AHMED was born in Chattogram, Bangladesh. He is currently pursuing the B.Sc degree in electrical and electronic engineering (EEE) with Hajee Mohammad Danesh Science and Technology University, Dinajpur, Bangladesh. He developed an early fascination with the dynamic field of semiconductor physics. His research interests include solar cell design, renewable energy, and solar PV systems.

ABDULLAH AL MAMUN was born in Jashore, Bangladesh. He is currently pursuing the B.Sc. degree with the Department of Electrical and Electronic Engineering, Hajee Mohammad Danesh Science and Technology University, Dinajpur, Bangladesh. His research interests include renewable energy, power electronics, and machine control.

MD. NURALAM HOWLADER received the B.Sc. (Engg.) degree in electrical and electronic engineering from Hajee Mohammad Danesh Science and Technology University, Dinajpur, in 2022. His research interests include the development of electrical power and energy conversion systems, renewable energy systems, electrical energy storage, smart grids, sustainable technologies, machine learning, smart grid and energy management, advanced power electronics, photovoltaics, thin film solar cells, perovskite solar cells, solar energy materials, and emerging semiconductor technologies.

TARPAN PAUL received the bachelor's degree in electrical and electronics engineering (EEE) from the Mymensingh Engineering College, Mymensingh, in 2017. He is currently pursuing the master's degree with the Institute of Information and Communication Technology (IICT), Dhaka University of Engineering and Technology, Gazipur, Bangladesh. His current research interests include underwater wireless sensor networks, the Internet of Underwater Things, and renewable energy.

MD. MOTIUR RAHMAN TAREQ received the B.Sc. (Engg.) degree in electrical and electronic engineering from Hajee Mohammad Danesh Science and Technology University, Dinajpur, in 2018. He is currently pursuing the M.Sc.Eng. degree in electrical and electronic engineering with the Khulna University of Engineering and Technology, Khulna, Bangladesh. He is employed as a Lecturer with Hajee Mohammad Danesh Science and Technology University. His research interests include renewable energy, especially solar cells, photonic crystal fiber, and machine learning.

MD. SAZEDUR RAHMAN (Graduate Student Member, IEEE) received the B.Sc. degree in electrical and electronic engineering from the Khulna University of Engineering and Technology, Khulna, Bangladesh, in 2020, where he is currently pursuing the M.Sc. degree in electrical and electronic engineering. He is employed as a Lecturer at Hajee Mohammad Danesh Science and Technology University, Dinajpur, Bangladesh. His research interests include the development of area-time efficient elliptic curve cryptography using FPGA, efficient usages of solar panels, fundamental study of material science, and fabrication of micro or nano-structured surfaces. His awards and honors include the Dean's Award from the Khulna University of Engineering and Technology.

MD. MIZANUR RAHMAN received the B.Sc. degree in electrical and electronic engineering from the Rajshahi University of Engineering and Technology, Rajshahi, Bangladesh, in 2012. He was a Lecturer with the Department of Electrical and Electronic Engineering, Hajee Mohammad Danesh Science and Technology University, Dinajpur, Bangladesh, from 2013 to 2016, where he has been an Assistant Professor, since 2016. His research interests include renewable energy, smart grid systems, and power system stability.